Transition Metal Ion Ensembles in Crystals as Solid-State Coherent Spin-Photon Interfaces: The Case of Nickel in Magnesium Oxide

E. Poem();•• S. Gupta,21. Morris,3 K. Klink,[3] L. Singh,[1] T. Zbong,2 S.S. Nicley,[4•5] J.N. Becker,3.S and
0. FirstenbergG[1]

[1] Department of Physics of Complex Systems, Weizmann Institute of Science, Rehovot 7610001, Israel
[2] Prizker School of Molecular Engineering, The University of Chicago, Chicago, Illinois 60637, USA
[3] Department of Physics and Astronomy, Michigan State University, 567 Wilson Road, East Lansing, Michigan 48824, USA
[4] Department of Electrical and Computer Engineering, Michigan State University, 428S. Shaw Lane, Room 2120, East Lansing, Michigan 48824, USA
'Coatings and Diamond Technologies Division, Center Midwest (CMW), Fraunhofer USA Inc., /449 Engineering Research Court, East Lansing, Michigan 48824, USA

(Received 3 January 2023; revised 23 June 2023; accepted 21 July 2023; published 30 August 2023)

We present general guidelines for finding solid-state systems that could serve as coherent electron-spin-photon interfaces even at relatively high temperatures, where phonons are abundant but cooling is easier, and show that transition-metal ions in various crystals could comply with these guidelines. As an illustrative example, we focus on divalent nickel ions in magnesium oxide. We perform electron-spin-resonance spectroscopy and polarization-sensitive magneto-optical fluorescence spectroscopy of a dense ensemble of these ions and find that (i) the ground-state electron spin stays coherent at liquid-helium temperatures for several microseconds and (ii) there exist energetically well-isolated excited states that **can couple to two ground-state spinsublevels via optical transitions of orthogonal polarizations. The latter implies that fast coherent optical control over the electron spin is possible. We then propose schemes for optical initialization and control of the ground-state electron spin using polarized optical pulses, as well as two schemes for implementing a noise-free broadband quantum optical memory at near-telecom wavelengths in this material system.**

DOI: 10.1103/PRXQuantum.4.030329

I. INTRODUCTION

Quantum communication and networks require coherent coupling between traveling qubits, carrying the quantum information, and stationary qubits, which can act as memories and processors, storing and manipulating the quantum information [I]. Photons at wavelengths in the telecommunication bands are arguably the best traveling qubits, as they have very low loss probability and can maintain their coherence over long distances in standard telecom fibers. Solid-state defect spins [2,3] are promising stationary qubits, as they are embedded in a miniaturizable platform. At room temperature, they can have coherence times as long as milliseconds [4] for electron-spins and tens of minutes [5] for nuclear spins. This only improves at low temperatures, where coherence times of up to seconds [6] and hours [7] have been achieved. One of the outstanding challenges toward the realization of optical quantum networks is the coherent coupling of telecom photons and solid-state qubits. For defect spins, this would mean the coherent coupling of light and spin.

As light (at optical wavelengths, in the far field) directly affects only the orbit of the electron but not its spin [8] and even less so the nuclear spin, any spin-photon coupling has to be mediated by additional internal interactions within the quantum system. For electron spins, this would be the relativistic effect of spin-orbit (SO) coupling. For nuclear spins, one also has to consider the hyperfine coupling. In this work, we discuss the case of electron-spins, where this leads to the two following requirements.

First, to coherently couple light at a certain frequency to an electron spin at a given temperature, i.e., to coherently transfer quantum information between them, there should exist an excited state at that frequency (with respect to the ground state) in which the SO-coupling rate is much

---

- **eilon.poem@weizmann.ac.il**

faster than the total (homogeneous and inhomogeneous) decoherence rate of the ensemble at that temperature. This also includes cases where only a part of the ensemble is addressed by, e.g., spectrally selective optical pumping to a dark state [9] or by using light with a narrower spectrum than thatof the full ensemble [JO], where the relevant decoherence rate would be that of the addressed subensemble and not of the entire ensemble. Further, the duration of the optical field in the material should be long enough to allow for the SO interaction to act but still shorter than the optical coherence time of the relevant ensemble. While some coherent effects have been previously seen in both ensembles [11,12) and single spin centers [13) when using pulses shorter than the SO-coupling time, these were due to coherent orbit-photon coupling and not to coherent spin-photon coupling.

For ensembles of spin defects, the typical total broadenings of the optical transitions are between I00 MHz and JOO GHz, at low temperatures [2,14). Thus, coherent spin-photon coupling using the entire ensemble requires *SO coupling at the gigahertz-to-terahertz scale.* At higher temperatures, this may increase further.

Second, at operating temperatures of a few kelvin and above, where the cooling power of existing cryostats increases dramatically and their complexity and cost decrease dramatically [15), phonon modes of the defect and the host crystal are usually no longer frozen, as at millikelvin temperatures [2). Thus, the ground-state spin should couple to the electron orbit as little as possible, as such coupling would expose it to decoherence due to the interactions of the orbital degree of freedom with phonons. One known way of achieving this exists when the quantum information is encoded on nuclear spins. In that case, one can apply a strong magnetic field and shift the energy of neighboring electron-spin states enough to quench two-phonon scattering processes even at few-kelvin temperatures [16-18).

An alternative solution, which does not require high magnetic fields or subkelvin temperatures and applies to electron-spin qubits, is to use an electronic system with a *ground-state orbital singlet,* and therefore zero effective orbital angular momentum and zero first-order SO coupling in the ground state.

The tension between these two requirements can be illustrated with a few example cases.

The first case is that of ensembles of nitrogen-vacancy (NV-) centers in diamond [19). While these ensembles comply with the second requirement (a $^3A_2$ ground-state manifold), theydo notcomply with the first (about 30-GHz inhomogeneous broadening and only about 3-GHz SO coupling within the ^3E excited-state manifold). Therefore, they have excellent spin properties [4,6) but only incoherent spin-photon coupling (coherent spin-photon coupling was achieved only at low temperatures, for single NV-centers [13,20-24) or for very small subensembles [10)).

The second case includes both negatively charged group-IV-vacancy centers in diamond [25) and commonly used rare-earth-ion ensembles [2,16-18,26), such as Pf3+, Eul+, Yb^{3+}, or Er3+. These systems feature orthogonal challenges to the NV- center, as they have strong SO in the excited state but an orbital multiplet ground-state manifold. Therefore, while they may support high-temperature coherent spin-photon coupling, in the absence of very high magnetic fields their ground-state spin quickly decoheres above liquid-helium temperatures. For example, the electron-spin coherence time of Yb^{3+} in Y$_2$SiO$_5$ at 9 **K** is 2 μ,s, limited by fast two-phonon spin relaxation [27).

The third example case is that of the three known rare-earth ions with zero orbital angular momentum (i.e., in an S state), Gd^{3+} [28,29), Eu^{2+} [30,31), and To^{4+} [30,32), and the S-state actinide ion Cm^{3+} [33). These ions comply with both requirements and indeed exhibit very narrow spin distributions and optical line widths, some of them even up to room temperature. Unfortunately, the first three have optical transitions only in the ultraviolet, and the last one, while having transitions in the visible, is radioactive. This makes them less suitable for optical-communications purposes.

In contrast to the above examples, transition-metal ions, even in high-symmetry lattice sites of cubic crystals [34), can comply with both requirements while having optical transitions at infrared or even telecom wavelengths. First, due to their relatively large atomic number, the SO interaction is usually on the order of a few terahertz (similarly to the case of rare-earth ions). Second, due to the effectof the crystal field, which can be much stronger than in rare-earth ions, there are multiple cases with ground-state orbital singlets (similar to the NV-). This happens whenever the highest set of degenerate single-electron orbitals is half filled. For weak crystal fields, forming high-spin configurations, the only relevant configuration is $d5$ (in analogy to the/^{7} configuration of the S-state rare-earth ions). For stronger crystal fields, however, where low-spin configurations form, there are more options. For cubic sites, these include $d8$ and $d3$ ions in octahedral sites and $d2$ and d^1 ions in tetrahedral sites. Of these, the configurations with an even number of electrons have an $S = 1$ ground state, while those with an odd number have an $S = 3/2$ ground state. While some transition metal ion systems have been investigated in the context of quantum information processing [3 38), the only such system having an orbital singlet ground state that has been investigated in this context, to the best of our knowledge, is Cr'+ in GaN and SiC [39,40), which has a $d2$ configuration in a tetrahedral site. It indeed displays infrared emission (around 1090 nm) and a coherent ground-state spin up to at least 15 **K.** This spin could potentially be coherently controlled optically, though, to the best of our knowledge, this has not been demonstrated yet.

Here, we focus on another such example:divalent nickel ($Ni^{2}+$) substituting for a magnesium ion in magnesium oxide (MgO). It hasa $d8$ configuration and due to the octahedral geometry of its site, its ground state is an orbital singlet and spin triplet. This system has been very thoroughly studied in the pastfew decades, both for fundamental characterization[41 2] and for applications, mostly as a potential gain medium for tunable and pulsed infrared lasers [6 5). Thespin-triplet nature of the ground state was already confirmed by electron-spin-resonance (ESR) studies over 60 years ago [41-43). The spin-lattice relaxation time (T1) has been measured to be as long as I ms at 3.5 **K** and 17 μs at 35 K for a magnetic field induced ground-state splitting of 9.2 GHz. Even longer times may be measured for smaller splittings, especially at the lower part of the temperature range (20 **K** and below), where the dominant process is single-phonon scattering, the rate of which scales quadratically with the spin splitting [47,48). Optical studies have revealed richemission and absorption spectra [41,45,49,51,59,60,65). In particular, the lowest-emission-energy zero-phonon lines (ZPLs) are at 1220 run and 1250 run, where the loss rate in a commercial optical fiber is approximately 0.4 dB/km, not much different than the approximately 0.3 dB/km loss rate in the O band (1310 run). Remarkably, these lines remain well separated up to temperatures as high as 150 K. The optical lifetime of these lines is very long, about 3.6 ms [64,65], up totemperatures of approximately I00 K. While this indicates a weak transition dipole moment, predominantly magnetic, due to the perfect solubility of NiO in MgO [61], optically dense ion ensembles could be readily made, compensating for the weak optical response of individual ions and enabling a strong collective response. Furthermore, as only 5% of the atoms in MgO made with natural isotope abundances have nonzero nuclear spin (due to ^{25}Mg), the spin dephasing rates due to nuclear spin-bath noise should be low and have been theoretically predicted to be below I kHz [66,67]. Importantly, like diamond [4], this material can bemade nuclearspin free by using isotopically purified precursors [68).

These compelling features lead us to reexamine this material system for use as a coherent spin-photon interface at above-liquid-helium temperatures. We experimentally investigate both the ground-state spin decoherence mechanisms and the spin structure of the excited state and show thattheyare compatible with terahertz-bandwidth coherent optical spin control even at temperatures exceeding that of liquid helium, estimated to go up to a few tens of kelvin.

The rest of the paper is organized as follows. In Sec. II, we describe the level structure of $Ni^{2}+$ in MgO, both that of the ground state and of the excited states, where for the latter we focus on the difference between the case of a weakly perturbed SO coupling and that of quenched SO coupling due to a strong dynamic Jahn-Teller (DJT) distortion of the excited-state orbitals [69]. In Sec. III, using ESR and temperature-dependent spin-echo (SE) measurements, weshow that for a high-density ensemble, the main decoherence mechanism is dipolar interaction between the ensemble spins. For a few gigahertz of ground-state splitting (induced byan external magnetic field), this interaction is already saturated at liquid-helium temperatures, leading to a decoherence time of 3 μs. In Sec. IV, we use polarization-sensitive magneto-optical fluorescence spectroscopy on the two ZPLs and show that the excited-state spin structure is indeed determined mostly by theSO interaction, since the DJTdistortion of the excited-state orbitals is weak. Following these findings, in Sec. V, we propose protocols for optical spin-state preparation, measurement, and manipulation, as well as fornoise-free optical quantum memories. Finally, in Sec. VI, we summarize our results and outline possible directions for future research.

U. LEVEL STRUCTURE

A. Ground state

The ground state of an $Ni^{2}+$ ion in an octahedral site of a cubic lattice(*Oh* symmetry group) contains twoelectrons (or, equivalently, two holes) occupying two degenerate *ea* single-electron orbitals (formed by the d,,_,,2 and d,2 *d* orbitals), as shown in Fig. l(a). *As* this is a half-filled shell, there is only one many-electron orbital. The total spin of the two electrons can be either O or I but the spin-I states have a lower energy. The ground state is therefore an orbital-singlet spin triplet, $^{3}A_{2g}$, thespin-orbit representation of which is T_{2}•. The effective Hamiltonian for this manifold is

$$Ha = \mu_{8} g f B \cdot S + S \cdot q(£) \cdot S + \mu_{8} B \cdot 8gs(£) \cdot S, \quad (I)$$

where S is the vector of spin-I operators, **B** is the magnetic field vector, **q(£)** is the strain-induced magnetic quadrupole moment, 8gs(£) is the strain-induced *g* tensor [70], and £ is the strain tensor. Here, μ_{8} is the Bohr magneton and is the ground-state *g* factor. The three spin states are degenerate at zero fields and strains. A constant magnetic field along the *z* direction splits the states via the Zeeman interaction [the first term in Eq. (I)]. Due to the second term in Eq. (1), local random strains (of a cubic lattice) can shift the $T2u,o$ state with respect to the $T2u,\pm 1$states to first order in the ratios of thestrain energies and the Zeeman energy. This inhomogeneously broadens the $T_{2.,1}$ ..., $T2u,o$ and the $T2u,o$ ..., $T2u,-1$ spin transitions. The same term can also split the $T2u,\pm 1$ states; however, only tosecond order instrain-to-Zeeman-energy ratio[70). This is because the relevant strain terms are off diagonal in the magnetic field Hamiltonian, such that their effect is quenched as the magnetic field becomes large, leading to a reduced broadening of the $T2u,1$ $T2u,-1$spin transition. The third term in Eq. (I) cannot shift the $T2u,o$ state with respect to the $T2u,\pm I$ states but can split the $T2u,\pm J$

states to first order. However, in MgO, for an applied magnetic field on the order of 100 mT (a few gigahertz *T2u,1* <-> *T2u,o* Zeeman splitting), this splitting is about 2 orders of magnitude smaller than the first-order shifts induced by thesecond term[43,7 73], keeping thebroadening of the*T2u,₁* <-> *T2u,-i* spin transition smaller than that of the *T2u,o* <-> *T2u,±1* transitions. The level splitting and broadenings are schematically presented in Fig. I(d). In Sec. Ill, we present ESR measurements of these inhomogeneous broadenings, as well as SE measurements of the homogeneous decoherence time at different temperatures.

B. Excited state

The first excited state of Ni^{2+} in MgO is composed of one hole in one of two *ea* single-electron orbitals and one bole in one of three *t₂a* single-electron orbitals (formed by the *d,,, dxz,* and *d:ryd* orbitals), as shown in Fig. l(b). Therefore, there are six possible two-electron orbitals. The cubic symmetry splits these six states into two orbital triplets, T*1a* and *T2a,* where the latter has a lower energy [45]. The spin state of the two electrons in the lowest excited-state manifold is again a spin-I triplet. Thus, the lowest excited-state manifold is $^3T_{2g}$, which contains nine states in total.

These states are coupled and split by the spin-orbit interaction. Its magnitude depends on the strength of the dynamic Jahn-Teller (DJT) coupling between the electronic orbitals and lattice vibrations, as the latter may affect the shapes of the orbitals and thus their effective angular momentum [69]. The effective Hamiltonian for the $^3T_{2g}$ manifold, in the presence of a magnetic field, is

$$H^e(\kappa) = H^e_{\rm so}(\kappa) + H^e_R(\kappa), \tag{2}$$

where κ = *3Err//i.wp,.*is the relative strength of the DJT coupling. It is proportional to the ratio between the electron-phonon coupling energy *Err* and the energy of the lowest phonon mode liwp,..

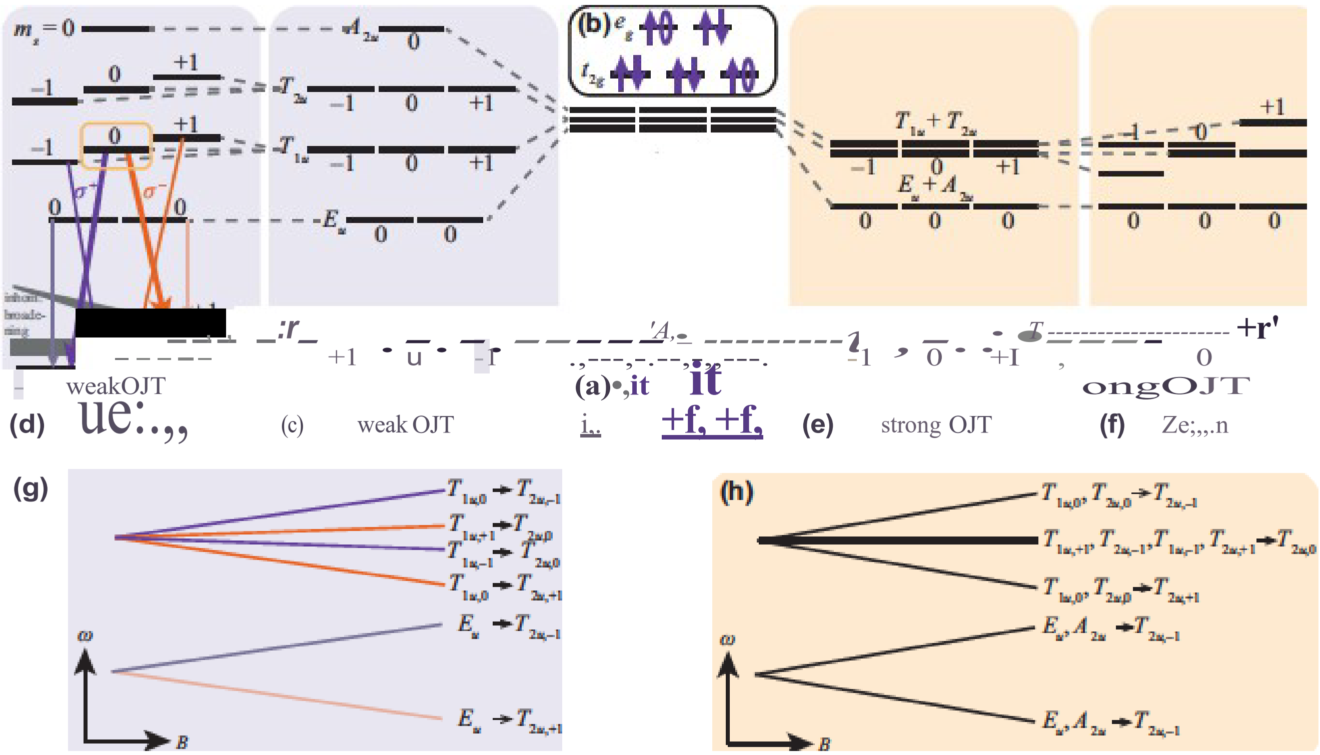

FIG. I. The energy-level structure ofNi^{2+}:MgO. (a) The ground-state electronic configuration. The 31Tows represent electrons and the ellipses represent holes. (b) The electronic configuration of the first excited state. (c) [(e)] The ground- and excited-state-level structures resulting from SO interaction in the presence of a weak [strong] DJT. (d) [(f)) The splitting of the ground- and excited-state spin sublevels in a magnetic field for weak [strong] DJT. The gray-shaded regions in the weak DJT ground state represent random-strain-induced inhomogeneous broadenings andtheir field dependencies. A polarized A system (orange rectangle) forms for weak DJT. Other relevant optical transitions are marked, where purple (orange) arrows represent *a+* - (a--) polarized transitions and fuded-color lines and 31Tows represent partially polarized transitions. (g) [(h)) The splitting of the optical-emission lines under a magnetic field (the field increases to the right) in Faraday configuration, for the case of weak [strong) DJT. The same color coding as in (d) is used. **The black lines denote unpolarized transitions. TE-polarized transitions are notshown.**

The zero-field Hamiltonian is (69)

$$H;,(K) = e-\bullet/2sL \cdot \mathbf{S} + [\mu.e-\bullet/2 + K1(\mathbf{K}))(\mathbf{L} \cdot S)2 + [p + \mu(l - e-\bullet/2) + K2(K))A, \tag{3}$$

where **L** **(S)** is the orbital (spin) angular-momentum vector operator and $A = L;S; + L;S; + L;S\}$ is a second-order cubic symrneby spin-orbit term. Here, both **L** and **S** are spin- I operators. The quadratic SO terms (the last two terms) arise from second-order perturbation theory applied to the full Hamiltonian (69). The energies K_1 and $K2$ are given by $K1 = $ <ifs^2//i.wpi,)e-•G(K/2) and $K2 =$ (gr{^{2}//uup,.)e-"(G(K)- G(K/2)), where $G(x) = J:dt (e' - l)/t$ (69,74). The magnetic field dependent Hamiltonian is

$$H^e_R = \mu_B(g_L e^{-\kappa/2}\mathbf{L} + g^e_e\mathbf{S}) \cdot \mathbf{B}, \tag{4}$$

where $g;$ is the excited-state g factor and gL is its orbital gyromagnetic ratio. Here, we have neglected the static strain shifts.

For weak DJT distortion, i.e., for $K < 1$, the "static lattice" SO structure survives and the ninefold-degenerate state space splits into four distinct energy levels (see Table I in Appendix A): a doublet *(Eu),* two triplets *(Tiu* and *T2u),* and a singlet *(A2u),* as shown in Fig. I(c). Out of these, the T_{1u} triplet contains one state, $T_{1u,o} =$ ^{1}/h(IT2a,1)ll),- IT2g,-1)l-l),) (marked in the figure), which mixes the I± I), spin states, each coupled to a different orbital. Note that the components of the total angular momentum in this state are ±2, which reverses the polarization-selection rules of the transitions from it to the $T2u,\pm 1$ ground states with respect to those expected from a state with zero total angular momentum. Nevertheless, these three states and the transitions between them manifest a polarized A system (Fig. 1(d)). Sucha level system enables the control of the$T2u,\pm 1$ground-state two-level system using polarized light (22,75-77).

For the opposite case of a strong DJT distortion, where $K \gg$ I, only the A term in the Hamiltonian ofEq. (3)survives and there are only two energy levels (see Table II in Appendix A): a triplet (composed of Eu and $A2u$) and a sextuplet (composed of T_{1u} and $T2u$), as shown in Fig. I(e). In this case, due to destructive interference between different states of thesame level, no A system can form (78) and coherent optical spin manipulation is prohibited (Fig. I(f)). lt is therefore crucial to distinguish between the weak and strong DJT regimes.

lf the absorption spectrum were to feature four distinct narrow lines, as is thecase for, e.g., Ni^{2+} in forsterite (79), the favorable weak DJT case would be clearly identified. However, only two of the observed absorption lines are narrow, while the rest are broad (45). This could be for one of two reasons: (i) the broad lines include the two remaining "static lattice" lines but mixed with high-energy vibrations (which are not included in theabove model); or (ii) the broad lines are purely vibrational lines and the two narrow lines are the result of a strong DJT distortion of the electronic levels.

In the literature, the common interpretation is that of weak DJT and some studies assign energies to the upper two electronic transitions [45,65). However, so far, this interpretation bas not been validated other than via a theoretical analysis of the possible vibrational modes ofNi^{2+} in MgO (52,53) and recent theoretical studies have questioned it (62). In Appendix B, we show that both thestrong and weak DJT cases can fit the observed spectra. Furthermore, cases of other transition-metal spin- I systems where only two of the four expected narrow absorption lines have been observed, namely y^{3+} in GaAs, GaP, InP (80-89), and ZnO (90), have been reported and strong DJT distortion bas beenshown to be the valid case for these systems. This was achieved by analyzing the magnetic field dependence of the absorption spectrum (83,90). For the case of Ni^{2+} in MgO, while magnetic circular dichroism has been probed in the past (54,55), no conclusion regarding the excited-state spin structure bas been drawn.

Figures l(g) and l(h) present the magnetic splitting of theoptical transitions forthe cases of weakandstrong DJT, respectively (see Appendix A). It is clearly seen that both the number of spectral components and their polarizations differ between the two cases, allowing for a clear distinction between them. lo Sec. IV, we present polarized optical magnetofluorescence spectroscopy measurements for the two lowest-energy ZPLs of Ni^{2+} in MgO, which unambiguously support the case of a weak DJT distortion, with K "" 0.I3 (see Appendix B).

III. GROUND-STATE SPIN COHERENCE

For the experiment, we use a 5 mm x 5 mm x I mm single-crystal MgO sample, cut along the (00I) planes and optically polished on the two large facets, grown by Goodfellow Inc. It was intentionally doped with 450-ppm (2.4 x 10^{19} cm-^{3}) of nickel (nominally) and had a nominal concentration of IO ppm of unintentional dopants. The sample was investigated as grown, with no further processing.

For ESR and SE measurement, thesample was placed in a 5.006-GHz aluminum microwave loop-gap cavity with a line width of I MHz. The cavity was mounted on the mixing chamber of a Bluefors LD250 dilution refrigerator reaching a base temperature of 8 mK. A three-axis vector magnet (AMI Model 430) was used to apply a magnetic field. A cryogenic amplifier (Low noise factory LNF-LNC0.3_14a) was used to preamplify the spin-echo signal, limiting the maximum microwave power to < I mW and the maximum temperature to 4 K.

The ESR spectrum measured at 4 K is presented in Fig. 2, with themagnetic field approximately aligned along

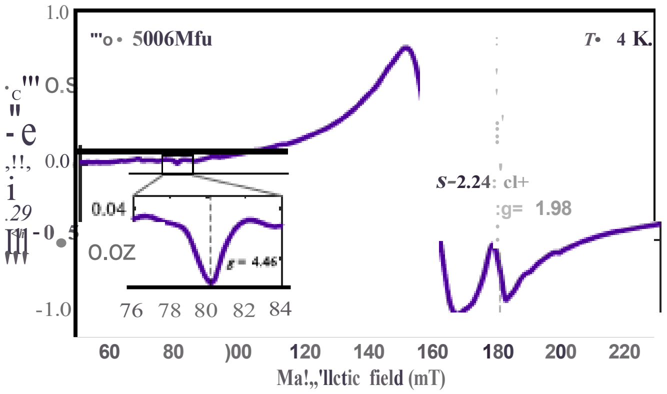

FIG. 2. The electron-spin-resonance (ESR) spectrum of the ground-state spin of Ni^{1}+:Mg0. The magnetic field was calibrated using the *c,3+* line at $g = 1.98$. The inset is an enlarge**ment of the spectrum around the*6m″*= 2 transition.**

the [100] axis. The relatively narrow feature around 180 mT ($g = 1.98$) is a well-known transition of cr3+ [9I]. We have verified the presence of cr3+ in our sample, also using fluorescence spectroscopy (see Sec. IV). We have used the known *g* factor of the cr3+ transition to calibrate the magnetic field. The dominant broad feature around 160 mT ($g = 2.24$) is related to Ni^{2}+. The measured *g* factor matches the known value of 2.214 [42] to the precision of our magnetic field calibration. Its width (peak to peak) is 13 mT, corresponding to 400-MHz line width. This large broadening is probably due to random strain introduced by the high concentration of dopants, limiting the inhomogeneous coherence time of the spin ensemble to approximately I ns. Similar widths have been measured previously and it is also known that high-temperature annealing reduces the width by about a factor of 2 [50]. We have not seen the "inverse line" previously observed in the center of the Ni^{2}+ line [42,50]. *As* this line was attributed to a homogeneous resonant cross-relaxation process [50], it could be that this process was quenched due to the low temperature in our experiment. We also could not observe the "double-quantum" line, due to a two-photon transition between the *T2u,-1* and *T2u,1* states [42,47,50], most probably due to our microwave-power limitation.

In addition to the strong Ni^{2}+ and cr3+ lines, the measured spectrum exhibits a small feature very close to half the magnetic field of the main Ni^{2}+ resonance, as shown in the inset of Fig. 2. We attribute this feature, which has the form of a Fano resonance ("bound state in a continuum" [8]), to the forbidden *ti.m,* = 2 single-photon transition between the *T2,J,-t* and *T2.,1* states of the Ni^{2}+ ground state. The transition becomes partially allowed due to strain [70]. The Fano shape, also seen in previous works [47], is most probably due to interference with the wide background coming from the *ti.m,* = I transition. The width of this line [the full width at half maximum (FWHM)] is 1.5 mT, corresponding to about 90 MHz and approximately 5-ns inhomogeneous coherence time. This narrow width (relative to the main transition) results from the lower strain sensitivity of the energy gap between the T_{2u}±*t* levels [70]. A similar ratio was alsomeasured for the double-quantum transition [42,47,50].

Next, we set the magnetic field to 141 mT, at the edge of the distribution, and measured the spin echo following excitation with two 500-ns-long pulses. The measured echo amplitude versus the time between the pulses, taken at 9 mK, is presented in Fig. 3(a). Most strikingly, we observe pronounced oscillations. The Fourier transform of this pattern is presented in Fig. 3(b). The main frequency component is at 385 ± 10 kHz, fitting the predicted 366 kHz of nuclear Zeeman splitting of ^{25}Mg at the applied field rather well. Additional components at the second and third harmonics of this frequency are also visible. The oscillations can therefore be explained *as* an electron spin-echoenvelope modulation (ESEEM) [92,93] caused by the coupling of the Ni^{2}+ electron-spin to the nuclear spins of neighboring ^{25}Mg atoms. The modulation frequencies exactly match multiples of the nuclear Zeeman splitting [marked by vertical dashed lines in Fig. 3(b)] and are not affected by any hyperfine coupling terms despite the strong modulation depth, in principle necessitating strong hyperfine coupling. This can beexplained by the zerospin component of the excited electronic state, limiting hyperfine coupling to the ground-state electron spin, which is fully occupied at the experiment temperature. However, *as* the nuclear spin state is still fully mixed at the experiment temperature, only transitions with the same ground-state

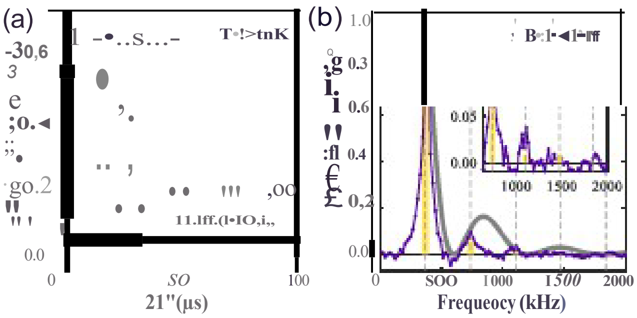

FIG. 3. Thespinechoat9mKand 141 mT.(a)Theamplitude versus the time between the twodriving pulses. The dotted lines **show the oscillation envelopes and their mean. The orange line is a fit of the mean of the oscillation envelopes to a biexponen**tial decay curve. The solid black line is the model fit (see text and Appendix C). The inset is an enlargement of the long-time range. (b) The frequency content of the measured echodecay. A wide background peaked at zero frequency has been subtracted The yellow bars are the relative oscillation amplitudes predicted by the ESEEM model (see text and Appendix C) multiplied by the instrumental spectral response (gray line). The inset is an enlargement of the high-frequency range.

nuclear spinand different excited-state nuclear spin would interfere and thus hyperfine coupling does not show up in the modulation frequency. Using the model presented in Refs. [92,93], adapted to the case of an initial (a final) electron-spin component of - I (0) and a nuclear spin of 5/2 (see Appendix C), we calculate the expected modulation frequencies and their amplitudes for the applied pulse and cavity bandwidths. These are presented as yellow vertical bars in Fig. 3(b).

The decay of the mean envelope of the oscillations can be fitted to a biexponential function [orange line in Fig. 3(a)], with a short decay time of J;$^{\text{shott}}$1 = 4.50 ± 0.03 μs and a long decay time of if•i!|= 109 ± 2 μs. As all the ESEEM modulation frequencies are equal to or higher than 366 kHz (the fundamental nuclear Zeeman frequency), the initial decay at a rate of *(2n.* 4.5 μs)-^{1} ::cs 35 kHz cannot come from ESEEM. Thus, toexplain theshape of the decay curve and its temperature dependence (see below), we consider three main dephasing mechanisms [94]: direct flipflop of neighboring spins within thesubensemble probed by the cavity; instantaneous diffusion dephasing due to the flipping of neighboring spins by the *n* pulse; and stochastic energy shifts ("spectral diffusion") of the probed spins due to flip flops of the entire ensemble [95,96). We neglect dephasing of the electron-spins due to nuclear spins (^{25}Mg and ^{61}Ni), *as* the product of their density and magnetic moments is much lower than that of the Ni^{2}+ electron-spin ensemble. We do include the dephasing of the ^{25}Mg nuclear spins themselves, as will beelaborated on below.

At low temperatures, the first two electron-spin dephasing processes usually dominate, as they involve resonant dipole-dipole interaction between close-by spins. However, in an inhomogeneous ensemble, some of the probed spins will have fewer probed-spin neighbors than others, leading to a distribution of decay times and to a biexponential decay curve [97]. Ingeneral, in thesubensemble of probed spins for which the immediate environment is of low density, the spectral-diffusion dephasing would make a more significant contribution to the total dephasing rate. However, at low temperatures the first two processes only weakly depend on temperature [94], while the spectral-diffusion dephasing, which depends on the number of spin pairs that can perform flip flop, vanishes at low temperatures [95). Thus, at very low temperatures, the short decay time is caused by the subensemble of probed spins withstrong instantaneous diffusion and direct flip flop and the long decay time originates from the subensemble in which these interactions are weak. One can model the low-temperature spin-echo trace by multiplying the calculated ESEEM trace by the fitted biexponential decay. As the nuclear spins also dephase (due mostly to static inhomogeneities [92]), one has to introduce a decaying envelope term also to the oscillation visibility (see Appendix C). The result of this model is presented in Fig. 3(a) by the solid black line. The extracted ^{25}Mg nuclear spin inhomogeneous dephasing time is -r;<•ucJ = 52 ± 2 μs.

The low-temperature short-time coherence strongly depends on the average density of the probed subensemble [96). This can be observed by scanning the field across the inhomogeneous broadening of the spin ensemble and probing thespin-echo amplitude for a fixed short time difference (here, 5.6 μs), *as* shown in Fig. 4(a). lt is clearly seen that the amplitude drops near the center of the distribution, where the density of probed spins is the highest, and thus most of the probed population would experience strong direct dephasing. The strong coherence peak at 180 mT is due toCr3+ ions, the density of which is much lower than that of the Ni^{2}+ ions.

As the temperature increases, the spectral-diffusion rate increases, first affecting only the lower density subensemble, until at a certain temperature it will dominate even over the direct processes in the denser subensemble, at which point the coherence decay will become monoexponential. Figure 4(b) presents the extracted long decay times versus temperature. The line is a two-parameter

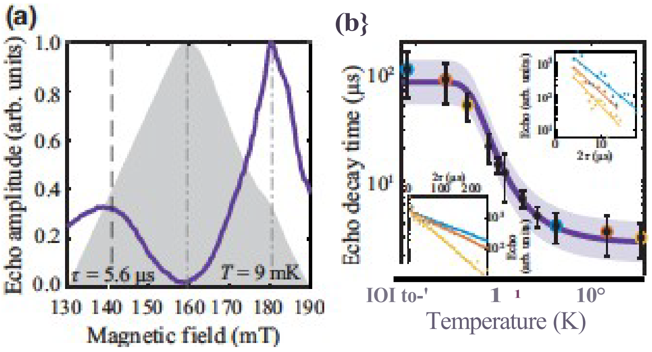

FIG. 4. The dependence of the spin coherence on the density and temperature. (a) The spin-echo amplitude (normalized to **its maximum value) at r = 5.6 µ.s and a temperature of 9 mK** versus the applied magnetic field The gray-shaded area is the integrated ESR signal, proportional to the defect density probed at each magnetic field value. The dash-dotted gray lines mark the peaks of the Ni^{2}+ and distributions. The black dashed line marks the field at which all time-dependent echo measurements were performed (b) The time dependence of the echo **signal versus the temperature. The dots are the echo-envelope** long decay times, extracted by exponential fils to the data. The error bars are the 68% confidence level of the fits. The solid line **is a two-parameter fit of the measured times to a model includ**ing the temperature-dependent spectral-diffusion dephasing rate **and an additional temperature-independent rate accounting for** the direct flipflopand the instantaneous diffusion processes (see Appendix D). The purple-shaded area marks the 68% confidence interval of this fit. The bottom-left (top-right) inset presents the measured echo signals versus the time delay (dots), for the three lowest (highest) temperatures, together with single.;,xponential functions fitted to the long-time range (solid lines). The colors correspond to the temperature, as marked in the main plot by the **solid circles.**

fit to a model including both a temperature-independent relatively weak component, due to instantaneous diffusion and direct flip flop in the low-density subensemble, and the temperature-dependent spectral-diffusion dephasing rate [95,96], the latter adapted to a spin-I bath (see Appendix D).

The spin decoherence rate saturates around liquid-helium temperature, yielding a coherence time of about 3 µ.s. At these temperatures, the coherence decay is indeed monoexponential [see the top-right inset to Fig. 4(b)]. As the rates of all the three dephasing processes we consider depend at least linearly on the ensemble density [95], there is a prospect of considerably prolonging the coherence time by using less dense ensembles. This, in combination with thermal annealing, could also considerably decrease the inhomogeneous broadening, bringing that of the $8m,$ = 2 transition to the level of a few megahertz, which would enable dynamical decoupling of the entire ensemble using nanosecond microwave or optical pulses. Note that this requirement could be considerably alleviated if picosecond or even femtosecond optical pulses could be used (see Sec. V). The ultimate limit is the spin lifetime, T_1, measured to be I ms at 3.5 K for a spin splitting of 9.2 GHz [47,48]. As, up to about 20 K, T_1 increases quadratically when decreasing the spin splitting [47,48], tens to hundreds of milliseconds may be within reach even for these rather high temperatures.

IV. OPTICAL SPECTROSCOPY

A. Emission spedrum

For optical fluorescence spectroscopy, we placed the sample in a closed-cycle low-vibration helium-flow cryostat (ARS CS204-DMX-20-OM). A diode laser at 660 nm (Thorlabs LP660-SF50) was used for excitation (into a vibrational side band of the $^3T_{1}a$ multiplet). The fluorescence was collected using an infrared-optimized, NA = 0.8 objective lens (Shibuya M ePLAN NIR IO0A) and analyzed by a 0.75-m spectrometer (Teledyne-Princeton Instruments SpectraPro HRS-750), equipped with a 300-g/mm grating (resolution limit of 30 GHz around 1250 om) and a lnGaAs CCD array detector (Teledyne-Princeton Instruments PyLoN IR) cooled by liquid nitrogen. Figure 5(a) presents the measured emission spectra at different temperatures. Two distinct lines, at 1220 nm and 1250 nm, dominate the spectrum, corresponding to the optical transitions from the first two excited states to the ground state. The (inhomogeneous) width of the lines up to temperatures of about 60 K is approximately I00 GHz, much narrower than the splitting between them, which is 5.28 THz. While the lines further broaden at higher temperatures (mostly homogeneously), it is clearly seen that they remain well separated up to temperatures as high as I50 K. The inset presents the emission spectrum around 698 nm, detected by the same spectrometer using a 1200-g/mm grating and a silicon CCD array detector (Teledyne-Princeton Instruments Blaze HR). The narrow emission line (18 GHz, close to the resolution limit of 15 GHz) of cr3+ [98] is clearly seen, supporting the identification of the ESR line at 180 mT (Fig. 2). By modulating the laser current and gating the CCD camera accordingly, we measured the time dependence of the fluorescence following the laser pulse and confirmed that the 1250-om fluorescence decay time in our sample is indeed approximately 3.6 ms, as previously reported for Ni^2+ in MgO [64]. Figure 5(b) presents the measured lifetime of the excited level versus the temperature. The inset presents an exemplary measurement. Very little change (approximately 2%) of the decay time is observed even up to IO0K [64].

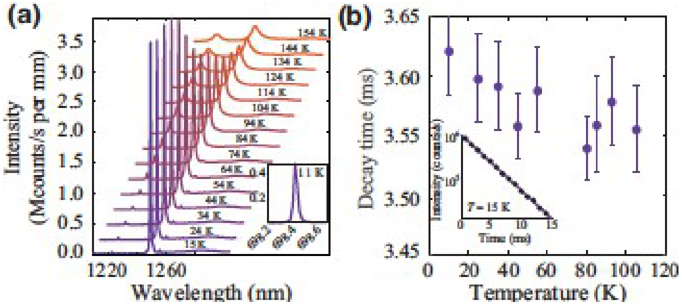

FIG. 5. The optical spectroscopy of Ni^2+:Mg0. (a) The temperature dependence of the emission spectrum. The inset (using the same units as in the main figure) shows the Cr3+ line around 698 nm. (b) The fluorescence decay time versus the temperature. The inset presents a characteristic fluorescence decay curve (semilogarithmic scale).

These features suggest that if one of the two excited electronic levels leading to the observed emission contains an SO-coupled state, the optical coherence time would not pose a limitation on the fidelity of optical spin manipulation performed using pulses of suitable duration (shorter than the optical coherence time, longer than the SO-coupling time) even at high temperatures (as long as the spectral width of the lines is smaller than the separation between them). We use magneto-optical spectroscopy measurements to verify that such a state indeed exists.

B. Magneto-optical spectroscopy

For performing polarized magnetofluorescence spectroscopy, we placed the sample in a closed-cycle helium cryostat (attocube attoDRY 2100), equipped ,vith a 9-T superconductingmagnet.Thesample temperature could be varied from I.7 K up to room temperature, independently of the magnet temperature, which was kept low and constant. A Ti:sapphire laser (Sirah Matisse CS) was used for optical excitation at 690 nm. Two sets of measurements were performed, one at I.7 **K** base temperature and the otherone at 60 K. Ineach set, themagnetic field was varied

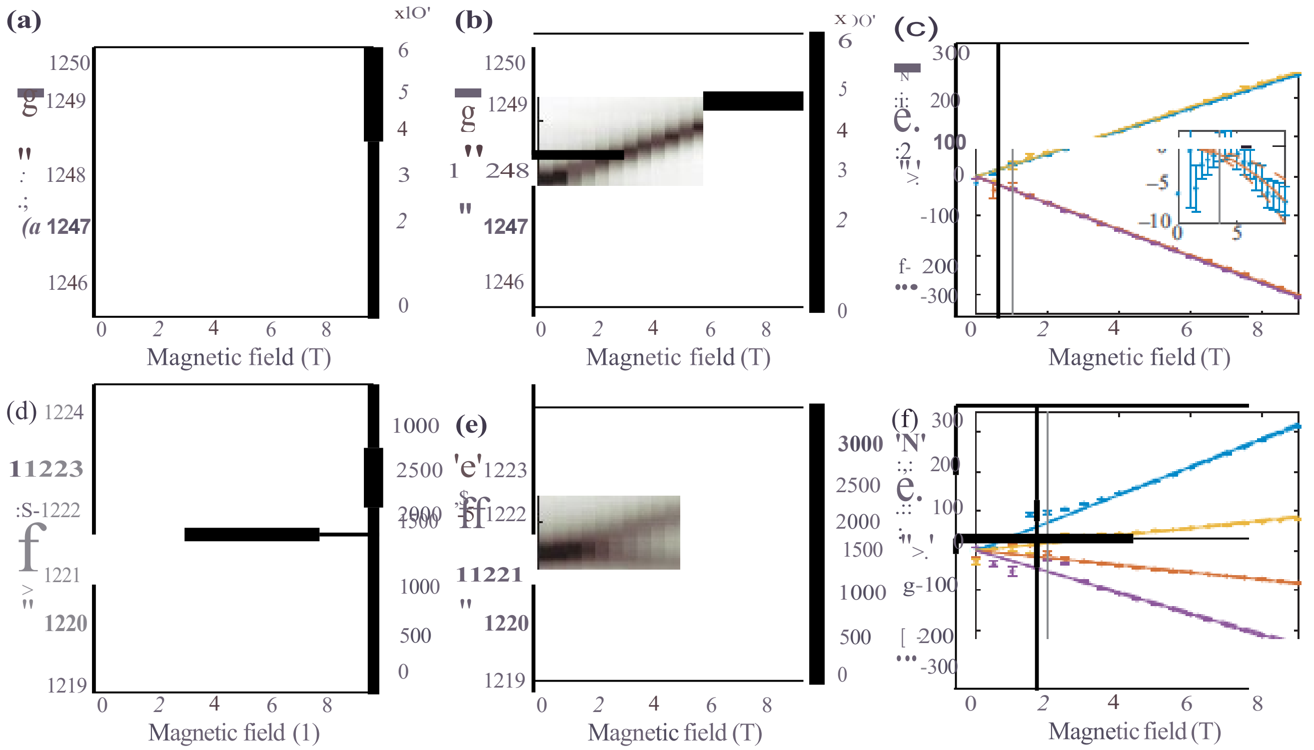

FIG. 6. The polarized magnetofluorescence spectroscopy measurements for determining spin-orbit coupling in the excited levels of Ni^{2+}:MgO. (a) [(b)) The measured spectra around 1250 nm for a+ [a-]circular polarization versus the applied magnetic field. (c) The line centers (dots) extracted from (a) and (b), together with linear regression fits (lines). The error bars present the errors in the line centers. For cases where only one spectral peak could be identified, only one point per data set is presented. The data points to the left of the vertical gray line were excluded from the linear regression. (d)-{f) The same as (a)-{c), for the 1220-nm emission. The inset in (c) presents the mean difference between the frequencies of oppositely polarized transitions of the same sign of the Zeeman shift versus the magnetic field *B*. At high fields, a significant difference from zero is seen. The solid line is a fit of Pr,-B^2 excluding the points to the left of the gray vertical line.

from O to *9* T and the emission spectrum was measured in two orthogonal circular polarizations. The emission was dispersed using the HRS-750 spectrometer, equipped with a 600-g/mm grating (resolution limit of I5 GHz around 1250 nm) and recorded using an electrically cooled CCD array camera (Teledyne-Princeton Instruments NIRvana HS). The first set focuses on the 1250-nm line (emission from the *Eu* level) and the second on the 1220-nm line (emission from the *Tiu* level). The 1220-nm emission was measured at an elevated temperature as it is extremely weak at lower temperatures, due to thermalization to the lowest excited state [see also Fig. 5(a)]. Figure 6 presents the polarized spectra for the two transitions.

At a high enough magnetic field, the 1220-nm emission splits into four fully polarized lines and the 1250-nm emission splits into two partially polarized lines, with a polarization degree (defined as the ratio of the difference between the intensities in the two polarizations to their sum) of about 50%. These patterns exactly match the prediction for the weak DJT case. In that case, the theory also predicts the Zeeman shifts of all emission lines (Appendix A).

In order to compare our measurements to the predicted Zeeman shifts, we fitted each of the measured fluorescence spectra to a double hyperbolic secant function and extracted the energies of the two peaks for every value of the applied magnetic field. These energies are presented in Figs. 6(c) and 6(1). We then fitted the magnetic field dependence of the peak energies to straight lines with a common origin. The best-fitted lines are also presented in the figures.

For the 1250-nm emission, the difference between the a+- and a- -polarized lines of opposite-sign slopes is predicted to be equal to the splitting of the ground state. That is, by dividing the slope difference by 2*μ,o,* one should obtain . In this way, we obtain a value of =2.242 ± 0.003. This value indeed closely matches the value directly measured using ESR. The theory predicts that the two *Eu* states should not split in a magnetic field, to first order. However, due to the (very small) magnetic field induced mixing of the *E.,,* state with the *T₁u,o* state, there should be a negative quadratic shift of its energy with the magnetic field [83]. Using second-order perturbation theory, the coefficient of this quadratic shift is given by P = -(*g; +gL)2141*1:i.21, where *gL* = *gLe-•/2* and 1:i.21 is the zero-field splitting between the *Eu* and *Tiu* states. Using the measured values of t:,.21 = 5.28 ± 0.02 THz and *g;* + *gL* = 1.33 ± 0.02 (obtained from the Zeeman splitting of the *Tiu* states, as shown below), we obtain Peale = -66 ± 2 MHz/T^2. While this effect is very small, we could directly measure it by looking at the difference between the energies of the *a*+- and *a*- -polarized lines having same-sign Zeeman shifts. At high enough magnetic fields, we could measure a significant (> 3o) deviation from zero, as presented in the inset of Fig. 6(c). It is also clear that the dependence of this deviation on the magnetic field is nonlinear. The solid line is a quadratic fit to the points for which *B* 3.5 T. The dashed lines present the 68% confidence level of this fit (mostly due to the uncertainty in the measured energy differences). From the fit, we obtain a value of *Pmeas* = -90 ± 35 MHz/T^2, which agrees with the calculated value to within the measurement error. A similar effect, though much larger, has previously been observed for yl+ ions in GaAs (83).

For the 1220-nm emission, the slope difference between the two outer lines is again only due to the ground state and is again predicted to be *2μ8Jf.*. We indeed extract a value of *J!,* = 2.22 ± 0.025, which is consistent with the value extracted from the *Eu* lines and with the ESR value. In addition to the linear slope, there should also be a small quadratic shift, common to both lines, due to the small magnetic coupling between the *T1u,o* and the *Eu,,* states. The magnitude of this effect should be the same as for the *Eu,,* state but its sign should be opposite, i.e., we expect a positive quadratic shift. However, as the signal here was much weaker than in the 1250-nm line, the accuracy of the assigned energies was lower, and we could not resolve this effect.

The slope difference between the two inner lines is related only to the splitting of the excited *Tiu* states and is predicted to be *a* = *μ8(fa* + If,). Assuming that the deviation of the electron *g* factor from the vacuum electron *g* factor, g_0 = 2.0023, is due to SO mixing alone (i.e., neglecting the crystal-field contribution) and taking into account only the closest T_{1u} state (which is that arising from the $^3T_1$ manifold), one obtains Jf,,lh = 1.84 (Appendix E). Together with the theoretical value of *gL, 1 1*〒 -0.47 (see Appendixes B and F), we obtain 0111 = *1.37μ9*. This predicted value is in a good agreement with the measured value of °'meas = (I.33 ± *0.02)μa*. An even better agreement may be obtained if the effects of the crystal field on the *g* factor were taken into account (99].

V. PROPOSED PROTOCOLS

Having established that the $^3T_2$ excited states of Ni^{2+} in MgO involve unquenched terahertz-level SO coupling and can thus mediate fast spin-photon coupling, in this section we present several protocols for optical control of the ground-state electron spin.

A. Spin-state preparation and measurement

Figure 7(a) presents the polarization-selection rules between the ground-state manifold and the two lowest excited-state manifolds, where the definitions of the polarizations with respect to the magnetic field and crystal axes are presented in Fig. 7(b) (see also Table I in Appendix A). These selection rules allow for polarization-based spin state preparation. Figure 7(c) presents the basic principle: excitation with a defined polarization leaves one of the three ground-state spin sublevels uncoupled to the excitation field. If the lifetime of this state is longer than the decay time from the excited state, most of the population will eventually accumulate in this state.

While the nonradiative decay from the *Tiu* to the *Eu* excited states is fast even at low temperature (as is evident from the thermalization of the excited-state population; see Fig. 5(a)], the decay from the *Eu* excited state to the T_{2u} ground states takes a few milliseconds, even at high temperatures (Fig. 5(b)). As the ground-state spin lifetime has been measured to be on the orders of milliseconds only at temperatures of a few kelvin [48], the standard optical pumping (Fig. 7(c)] may not work at higher temperatures.

There are at least two solutions to this problem. One is to use the fact that the *Eu* state is long lived and use it as a shelving state that stores the unwanted spin population while coherent operations are performed on the population that remains in the ground state, which is only of the desired spin state. For this, the polarized optical field should transfer all the unwanted population to the excited state before it decays. This can be achieved using an ultrafast optical *n* pulse, resonant with the 1220-nm transition *(T2u Tiu)*. In order to transfer the entire population, the excitation has to be coherent. This means that the pulse bandwidth has to be much larger than the optical line width (approximately I00 GHz). However, in order to not involve the *Eu* levels, which will spoil the polarization-selection rules, the pulse spectrum has to be narrower than the energy difference between the *Eu* and *Tiu* spectral lines (5.28 THz). An approximately I THz wide pulse, i.e., of a few hundred femtoseconds duration, would fit this range. One down side of this solution is that one decreases the optical density (the effective defect density) by a factor of 3 (as only a third of the defects are left in the ground state). Further, the shelved population is in a random spin state, making it a source of spectral-diffusion noise.

The second solution may overcome these two issues. As shown in Fig. 7(d), a second pulse, introduced after all the excited population has decayed into the *Eu* state, at a frequency matching the transition from the shelving *Eu* state to a phonon side band of the ground state, would stimulate the transition of the shelved population to the phonon

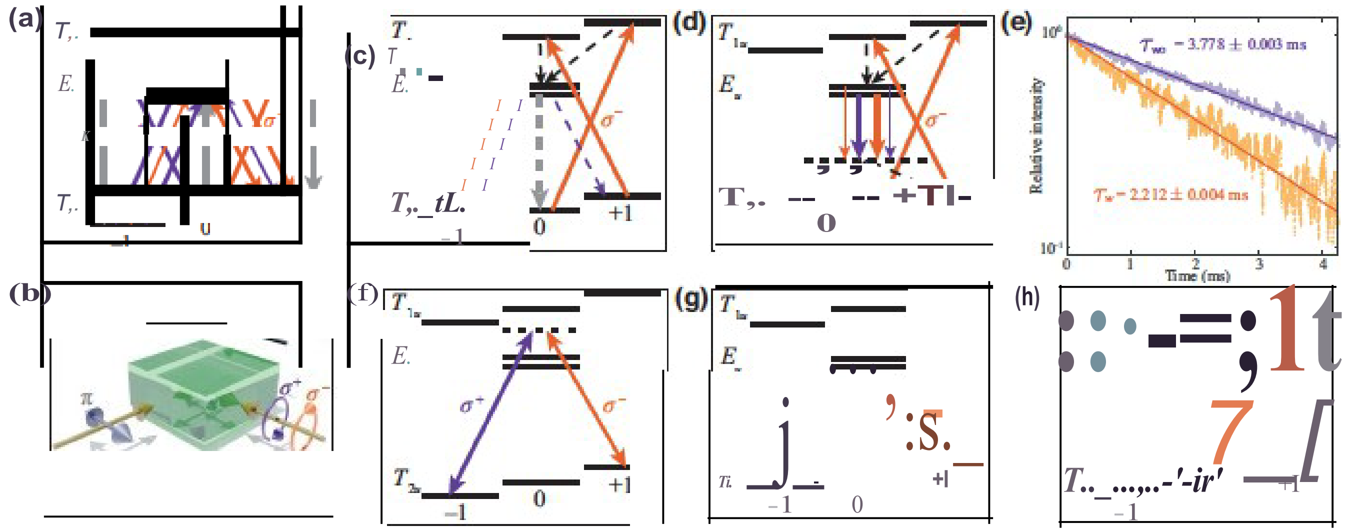

FIG. 7. The optical spin preparation, measurement, and control schemes. (a) The polarization-selectionrules foroptical transitions between the ground-state manifold, *Tu.,* and the first two excited-state manifolds, *E.* and *T1..,.* The purple, orange, and gray arrows represent transitions in *a+, u-,* and ,r polarizations, respectively. The widths of the arrows represent the strength of the transitions (see also Table I in Appendix A). (b) The geometry of the exciting optical beams with respect to the crystal axes and the applied magnetic field (c) Polarized optical pumping to the*Ti..,-1*state.Thedashed purple, orange, and gray (black) lines indicate spontaneous (non)radiativedecay. Similar schemeswith different pump polarizations allow pumping to the other twoground states.(d) The pulsed-state preparation. Here, the pumping is done using" pulses (e.g., of,,--polarized light) that transfer all undesired state population to the upper excited state. From there, all this population quickly decays to the lower excited state. It can either be shelved there for the lifetime of the lower excited state or it could **be** forced down to a phonon side band, which then quickly decays to the ground state. In **the latter case, to achieve full spin-state polarization, the process has to be repeated a few times. (e) Fluorescence decay curves without** (purple) and with (orange) the introduction of laser light at the phonon side band. A clear increase in the decay rate is observed. (f) [(g)] The coherent optical arbitraryspin rotation on the{T2u,1, *Ti.,-il* qubit spaceusing a polarized pulse around the T1. [£.]transition. (h) The coherent optical arbitrary spin rotation on the{T2.,1, *Ti.,ol* qubit space.

side band. From there, the population would quickly decay back to the ground state. Repeating the shelving and stintulating pulses a few times would result in most of the population being pumped into the ground state decoupled from the shelving pulse, in a similar manner to standard optical pumping.

To test the feasibility of this "stimulated optical pumping" concept, we introduced about 0.5 W of laser light at 1319 run (Sanctity Laser SSL-1319-1500-IOTM-D-LED) during the decay of the population after its excitation by the 660-run pulse. Figure 7(e) presents the fluorescence decay with and without the addition of the 1319-run laser. A clear decrease in the fluorescence decay time is observed, indicating the stintulation of population decay from the shelving state. The use of a cw laser, however, is inefficient, as only a small part of the phonon side band is used and the added power heats up thesample. The use of an ultrashort pulse for the stintulated de-excitation should solve these issues.

For optically measuring the spin state, one can turn on the polarized pumping light at 1220 runagain and monitor the resulting fluorescence at 1250 run. As for each of the three polarizations *(a+, a-,* and 1r), one of the three spin states is uncoupled from the polarized pumping field, the fluorescence intensity will be inversely proportional to the population of that state. The combined infonnation from all three measurements would thus yield the populations of all three states.

B. Coherent spin control

The polarized A systems present in the level sbucture allow for polarization-based full coherent control of the spin states using short optical pulses. Figures 7(1) and 7(g) present the relevant transitions for coherent control of the {T2u,1, T2v,-1} qubit manifold, through the *T1u,o* state or the *Eu* states, respectively. In the latter case, the couplingpaths through the two *Eu* states destructively interfere only partially, still enabling control. In both cases, the control pulse can be off resonance or near resonance, whereas in the latter case the pulse spectrum should be much wider than the line width of the relevant transition. The axis of rotation in the Bloch sphere is determined by the pulse polarization. The angle of rotation about this axis is determined either by the intensity of the pulse (off-resonant pulse) [100) or by the delUning of the pulse (near-resonant pulse) [IOI); in the latter case, the intensity is set to create a full 21r rotation, ending back at the ground state [75). Figure 7(h) shows the transitions employed to control the{T2.,1, *T2u,o)* qubit manifold. As they involve both *a* and rr polari7.ations, they have to be applied from orthogonal directions [Fig. 7(b)]. A similar arrangement with the opposite *a* polarization would drive the{T2•0, *T2._i)* qubit manifold. Here too, both near- and off-reso ance'control pulses may be applied.

C. Noise-free quantum memory

The ability to optically prepare and coherently control their spin state, combined with the near-telecom optical transitions and the possibility of creating high-optical-density ensembles, naturally suggests the application of divalent nickel-ion ensembles in MgO as quantum optical memories [102, I03). The quantum memory scheme most suitable toa medium with a large broadeningof theexcited state is the far-detuned Raman scheme [104). The optical cooperativity *C* of the system, which governs the memory efficiency [78], can beestimated using the transition dipole moment of the *T2.* B- r,. transition, 3.4 x 10^{-32}C.m,as derived from the oscillator strength of 4 x 10^{-7} [45]. We assume a density of2.4 x 10^{18} cm^{-3} (10 times lower than the density of the current sample), a detuning of200 GHz, and a waveguide 5 mm in length with a cross section of 5 x 5 μ,m^2. For control pulses of I μ,J, which are readily produced bystandard optical parametric amplifiers, we obtain *C* "" 2, indicating a total storage and retrieval efficiency of $C^2/(I+ C)^2$ ""45% [104). Thus, it seems that efficient Raman storage should be possible using realistic parameters. Furthermore, much higher cooperativity, *F* x *C,* and hence higher efficiency, can be obtained by adding an optical cavity with moderate finesse *F* [105-107], e.g., by using a ring-resonator structure or imprinting Bragg mirrors onto the waveguide.

One prevalent source of noise in a Raman memory scheme is due to four-wave mixing [108). This is the case when the control field couples to the full ground-level manifold and not only to the empty ground state, a situation aggravated at detunings larger than the ground-state splitting. However, ina Raman memory based on a polarized A system, a polarized control field couples only to a single ground state and thus four-wave-mixing noise is suppressed [77,78).

A second source of noise is the leakage of control light into the signal channel. When the signal and control are oppositely polarized, they can be separated by their polarizations. Usually, however, this is not enough, and a second separation mechanism, such as spectral filtering, is invoked [107-11I). This would be possible here only if the spectrum of the control pulse is narrower than the ground-state splitting but that would limit the bandwidth of the memory. Furthermore, tight spectral filtering usually lowers the efficiency of the memory. Here, we propose to replace spectral filtering with spatial filtering, by introducingan angle between thesignal and control modes. This is possible as, in contrast to warm atomic vapors, here the emitters do not move during storage and cannot create any motional dephasing due to signal and control wave-vector mismatch [I 12,113). Figure 8 presents two polarized Raman-memory schemes with an additional spatial-mode mismatch, applicable in the Ni^{2+} :MgO system.

The first scheme, described in the top three panels of Fig. 8, uses the *a*+ -polarized transition *T2.,1* B- *T1.,0* for the signal and the *a*- -polarized transition *T2u,-I* B- *T1.,0* for the control, where the ensemble is first prepared in the T2.,1 state. As shown in Fig. 8(a) (top), while the control field propagates along the magnetic field (setting the quanti7.ation axis), the signal field is at a small angle with respect to it. As shown in Fig. 8(b), this scheme is based on the {*T2.,1, T2u,-tl* qubit system. As shown in Fig. 2, while the relevant spin transition is narrower than that of the {T2.,1, T2.,0J qubit system, it is still considerably broadened. However, most of this broadening is due to inhomogeneous strain distribution, which could be mitigated by using a spin-echo sequence (and, generally, would be narrower in annealed samples [50]). Figure 8(c) presents a possible way to introduce the echo pulses optically. This could be done using a vertically polarized pulse near the *Eu* resonance, flipping between the*T2u,1* and T2v,-1 states. As shown in Fig. 8(a) (top), this pulse could potentially be applied from theside of thesample, perpendicular to the control and the signal, to minimize scattering into the signal mode, but it could also be applied along their direction, as it could rather easily bespectrally filtered out. Figure 8(a) (bottom) presents a possible pulse scheme including two rephasing pulses between storage and retrieval, where the time between the memory control pulses and the rephasing pulses is r and the time between the two rephasing pulses is 2r. This scheme would retum the qubit state to itsinitial state in time for retrieval. This is similar to the "revival of silenced echo" (ROSE) quantum memory scheme [114], as in the absence of a microwave cavity, the spin echo between the two rephasing pulses would be very weak.

Figure 8(d) presents a second noise-free memory scheme. This scheme, in contrast to the first one, stores both polarization modes of the signal. As shown in Fig. 8(e), starting from the system initialized in the *T2.,0* state, arr-polarized control pulse stores an amitrarily *a*±-polarized signal in the *T2uo* - *T2* • 1 and the *T2uo* - *T2u-1* coherences. The rr-pol ed control pulse is lntrodu ed from theside, so despite being in thesame frequency as the signal, it can be separated by both polarization and spatial filtering. As thestorage coherences include the broad *T2.,0* state, here rephasing is critical. Fortunately, thesame two-pulse rephasing scheme as described above can be used here as well. As the *T2*u,1 and *T2u,-1* states are s,vitched, the phase dispersion ofboth *T2.,0* - *T2u,1* and *T2u,o* - *T2u,-1*

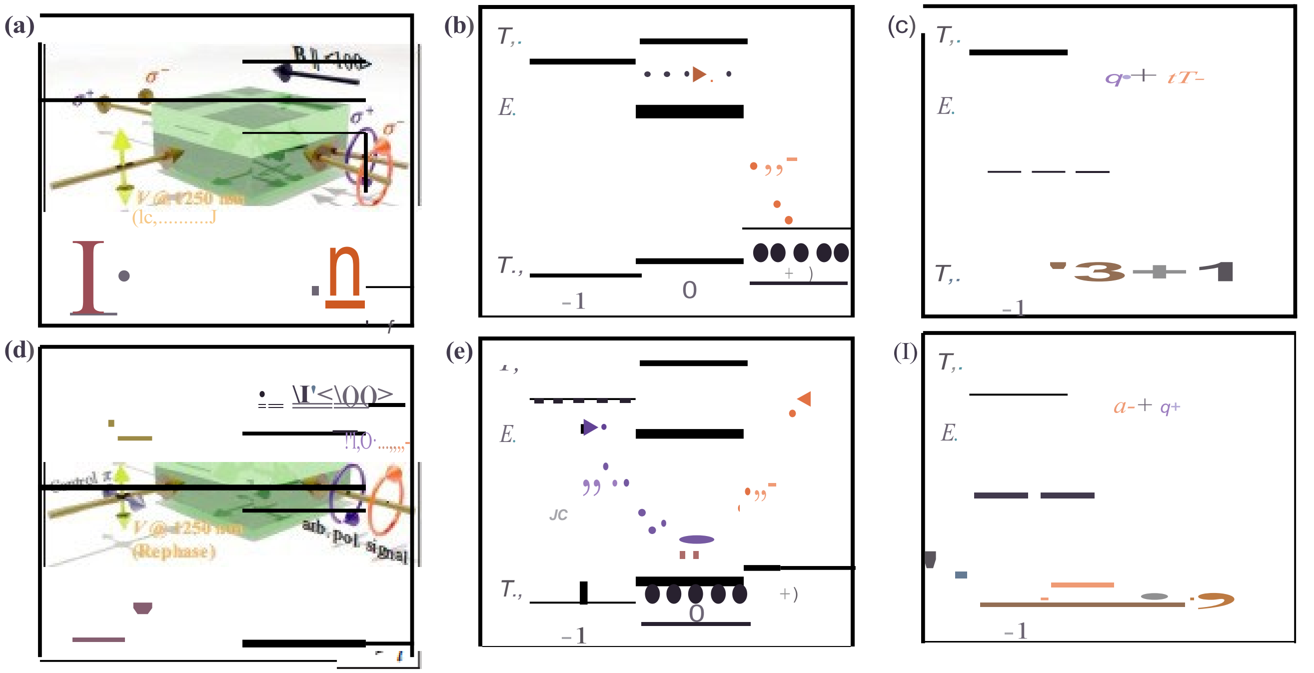

FIG. 8. Noise-free memory schemes. (aHc) Asingle-mode optionally rephased memory scheme. (a) The spatial configuration (top) and timing (bottom) of the optical pulses. (b) The storage of a a+ signal by creating a T2.,1- Ti.,-1 coherence in a medium initially prepared in the T2.,1 ground state, by a u- control field Asecond application of the control before the inhomogeneous dephasing time of the T2.,1- Ti.,-1 coherence would read the signal out. (c) A pair of rephasing pulses of vertical polarization (V)can be applied between storage and retrieval to cancel out the inhomogeneous dephasing, thus prolonging the memory time. (dHf) A polarization-conserving optionally rephased memory scheme. **(d)** The spatial configuration (top) and timing (bottom) of the optical pulses. (b) The storage of an arbitrarily polarized signal on the pair of coherenoes, Ti.,o - h,,1 andh,,o - T2.,-1, using arr-polarized pulse on a medium initially prepared in theTi.p ground state. **A** second application of the control before these two coherences decay would read the signal out. (f) Here too, a pair ofrephasing pulses of V polarization can be applied

coherences is reversed [Fig. 8(f)]. One down side of this scheme is that as the control comes from the side, the area it has to illuminate is much larger, necessitating a much larger pulse energy. This may be mitigated by embedding the waveguide into a planar microcavity, resonant with the control frequency, effectively enhancing the control power acting on the storage medium.

For the two memory schemes proposed above, the use of two rephasing pulses limits the applicability of such memories to cases where the required storage time is known in advance. This is the case for the synchronization of random events to fixed predetermined time bins. Nevertheless, the memory schemes could be adapted to cases where the release time bin is not predetermined. This can be done by setting the total rephasing time, 4r, to the minimum cycle time of the synchronized system, repeating the two-pulse rephasing sequence until retrieval is required, and then introducing the retrieving control at the end of the last rephasing cycle. This would amount to applying a Carr-Purcell-Meiboom-Gill (CPMG) sequence of variable length between storage and retrieval, and would thus have the added value of protecting the stored coherence from dynamical external noise (up to a frequency of 1/4r). Moreover, the applied pulse sequence does not have to be limited to CPMG. It could be any other periodic pulse sequence that can be terminated after an arbitrary number of periods. For example, one could apply a combination of the CPMG sequence and the Waugh-Huber-Haeberlen (WAHUHA) sequence [115], which protects both against external dynamical noise and against noise created by dipolar interactions within the ensemble, thus prolonging the memory time beyond the limit set by dipolar dephasing. This would alleviate the limit on the density of the ensemble, potentially further increasing the memory efficiency.

VI. CONCLUSIONS

We have introduced general guidelines for identifying electron-spin defects in solid-state systems that could coherently couple to light in the presence of significant optical decoherence, whether it is caused by inhomogeneous broadening in an ensemble, high temperature, or both. The two main requirements are an excited-state SO interaction faster than the optical decoherence and an orbital-singlet ground state. Following these guidelines, we propose to study transition metal ion ensembles in various crystals, and, as an example, we present the case ofNi^{2+} in MgO.

First, we perform ESR measurements of Ni^{2+}:MgO and extract both the inhomogeneous and homogeneous coherence times. In our sample, these are on the order of a few nanoseconds and a few microseconds, respectively, at liquid-helium temperature. Using temperature-dependent spin-echo measurement, we find that the main homogeneous broadening mechanism at this temperature is spectral diffusion due to dipolar interactions within the ensemble and that it is fully saturated. As the dephasing rate due to this mechanism depends on the density of the ensemble, the dephasing time could be prolonged by working with lower densities. Our particular sample is dense, containing approximately 450 ppm of Ni, and indeed lower densities would still be high enough to allow for efficient interaction with light. Alternatively, one could use designated dynamical-decouplingsequences to protect against dipolar dephasing or use optical-pumping techniques to polarize the spin ensemble. The ultimate limit is the spin lifetime, which, by working at small spin splittings, may be made as high as hundreds of milliseconds, even at temperatures as high as 20 K, on par with or even exceedingthe spin lifetimes of rare-earth ions at these temperatures [I I6]. Consequently, for single spin centers in dilute samples, where dipolar dephasing is negligible, our results infer that long coherence times could be achieved up to temperatures of several tens of kelvins, where low-cost Stirling coolers, with a high cooling power, can be used.

We could also detect ESEEM, which we attributed to ^{25}Mg nuclei in the host MgO crystal. This enabled us to extract an inhomogeneous nuclear spin coherence time of 52 μs at 9 mK. This may suggest that the homogeneous nuclear coherence time (which we have not measured in this work) may be very long, opening up the possibility of using the nuclear spin ensemble as a long-term quantum memory [I17-119].

Second, we perform magneto-optical spectroscopy measurements and verify that the excited states are indeed SO-coupled states, despite a weak DJT distortion of the electronic orbitals. This, combined with the observations of spectrally separated emission lines and an almost fixed fluorescence decay time up to higher than liquid-nitrogen temperatures, suggests that this system may be used as a coherent spin-photon interface at relatively high temperatures, limited only by the ground-state spin-coherence time. As discussed above, further work is required to measure this time versus temperature and establish the upper temperature limit.

Third, we propose detailed protocols for optical spin-state initialization and measurement and optical coherent spin control. Specifically, even when the spin lifetime is shorter than the excited-state lifetime, spin initialization is still possible using either shelving or pulsed stimulated decay. Based on these basic protocols, we then propose two noise-free high-bandwidth quantum memory protocols, possibly combining dynamical decoupling. While the first protocol is limited to single-mode storage, thesecond is for a two-mode polarization-preserving memory. Much more work is required in order to implement these protocols and to fully explore the potential of Ni^{2+} in MgO as a solid-state light-spin interface.

Moving forward, other transition-metal dopant systems could be explored. Some interesting candidates are eo^{2+} [120] and Ni^{3+} [121] (d^1 ions), or Fe6+ [122], Nb3+ [123] and Ta3+ [124] (d^2 ions), in tetrahedral sites. All of these are known to have optical transitions between 1550 and 1700 run, with weak or nonexisting DJT quenching. In addition, many other transition metal ion-doped crystals that match our general guidelines have not been studied at all.

We thus believe that this work can open the way to further investigations of transition-metal ions in crystals as a new family of materials with the potential of serving as the long sought after high-temperature coherent solid-state spin-photon interface, with major applications in quantum networks.

ACKNOWLEDGMENTS

E.P. would like to thank H. Bemien and D. D. Awschalom for facilitating his visit to the University of Chicago and for fruitful discussions. E.P. was supported in part by a grant from Fran Morris Rosman and Richard Rosman. E.P., L.S., and O.F. acknowledge support from the U.S.-lsrael Binational Science Foundation (BSF), the U.S. National Science Foundation (NSF), and the Estate of Louise Yasgour. S.G. and T.Z. acknowledge support by the National Science Foundation (NSF) Faculty Early Career Development Program (CAREER) (Grant No. 1944715), partial support by the University of Chicago Materials Research Science and Engineering Center, which is funded by the NSF under Award No. DMR-2011854, and the Army Research Office (Grant No. W9J l NF20I0296). l.M. was supported by an Alfred J. and Ruth Zeits Research Fellowship. J.N.B. acknowledges support by the Cowen Family Endowment at Michigan State University.

APPENDIX A: STATES AND POLARIZATION-SELECTION RULES

The three ground states can be described as spin-orbit product states, between the IA2g) orbital and the three spin states 11),, 10),, and I - l),. The excited states can be described as superpositions of spin-orbit product states between the three *T2a* orbitals IT2g,1), IT2g,o), and IT2g,-1) and the three spinstates.

TABLE I. The transition Zeeman shift in units of *μ.98* (left) and the relative transition probabilities in the three polarizations, *u+, n,* and*u-* (right), for the case of a *weak* DJT distortion. The orbital IT2g,') is abbreviated by *lk)t.*

		IA2g)l-l),	IA2g)IO),	IA2g)II),
E.,,	7201>,IIJ, + l-l)il-1),)	gf [½001	0 [OO OJ	-gf [OO½J
E.p	*(IIhi-I),+ 1-l)il I),)+ i10J1IO),	gf [OOtJ	0 [Of OJ	-gf [¼ 00]
T1.,,1	-(11)110), + IO)ilI),)	½(2gf +*ff,* + *KL)* [OO OJ	½<K:+ *Kt.HO* O½l	-½C2it - *ff,*- *Kt.)* [O½ OJ
T1.p	(II>i1l1, -1-lli1-t),)	*it*[½001	0 [OO OJ	-gf [OO½J
r,...-1	720-1)110), + 10)11-1),)	-½(2it +*ff,* + *KL)* [O ½ OJ	-½<K:+ *KL)* [½0 OJ	½c21t - *lf.* - *KL>*[0001

The optical transition probabilities between any excited state 1/), and ground state l1)g are given by

$$P^k_{ij} = |_e\langle j|D^k_M|i\rangle_g|^2, \tag{AI}$$

where , isthe magnetic dipole transition matrix in polari7.ation *k.* In the spin-orbit product basis used here, these matrices are given by

$$D^k_M \propto |k\rangle_l\langle A_{2g}| \otimes I_s. \tag{A2}$$

The state *lk)₁* is the T*2g* orbital state corresponding to the polari7.ation *k,* according to [125]

$$\{\sigma^+,\pi,\sigma^-\} \Leftrightarrow \{|T_{2g,-1}\rangle, |T_{2g,0}\rangle, |T_{2g,1}\rangle\}. \tag{A3}$$

The matrix *I,* isa unit matrix in the spin space and "®" is the Kronecker product. The proportionality constant is not important for the calculation of relative rates.

The ground- and excited-state wave functions, calculated according to the Hamiltonian in Eq. (3), the relative optical transition rates between them (in all polari7.ations), and the Zeeman-shift coefficient for these transitions are given in Tables Iand II forweak andstrong DJTdistortion, respectively. The tables neglect second-order magnetic coupling effects.

APPENDIX B: DJT MODEL AND THE ABSORPTION SPECTRA

The model in Eqs.(2)--(4) bas eight independent parameters: the electron-phonon coupling energy *Err,*the energy of the lowest phonon mode liwpi., the pure-electron-spin-orbit coupling parameters S,*μ,,*and *p,* the spin gyromagnetic ratios and *g;,* and the orbital gyromagnetic ratio - Below, we show bow the values of these parameters can be found from existing spectral measurements under two different interpretations, the weak and strong DJT distortion.

First, we find the relevant model parameters for the case of weak DJT distortion. Using the energy-level assignments from the literature [45,52,65], combined with our value for the ground-state spin *g* factor , one could find values for the first six parameters of the model [74], as detailed in Table III. The value of *g;* can be found from the value of S as shown in Appendix E and *gi* =- 1/2 can be calculated from the orbital structure, as shown in Appendix F.

The obtained values of *Err,* liwpi.S, and then yield *κ*= 0.13,K₁= 0.14 THz, andK₂= 0.15 THz, consistent with a weak DJT distortion.

For the second case, for which *κ* » I, the only relevant spectroscopic data is the splitting between the two narrow low-energy lines, Ll21. In this limit, *K1,K2* 0 and thus *Ll32::,:-:2{e-•12*. That is, it is becomes very small

TABLE II. The transition Zeeman shift in units of *μ.sB* (right) and relative transition probabilities in the three polarizations, *u+,* "• and *u-* (left), for the case of a *strong* DJT distortion. The orbital IT*2g,')* is abbreviated by *lk)t.*

		IA2g)l-l),	IA2g)IO),	IA2g)II),
E.,,	72(11)11I),+ 1-1>,i-1),)	gf [t O OJ	0 [O O OJ	*-gf* [OO½l
E.p	(11)i1-1), +1-1)tl I),)+ ilO>tlO),	gf [O O ¼J	0 [O j OJ	-gf [¼00]
A2.	:,;(II)ti-I),+ l-1)11I),) - IO)tlO),)	gf[OOiJ	0 [O i OJ	-gf [½ 00]
7i(T2.,1- T1.,-1)	IO>tll),	*gf* *-g;* [O I OJ	-,g;[O O OJ	*-gf* - *g;*[OO OJ
T1.p	72(11)11I), - 1-1>,i-1),)	gf [t O OJ	0 [O O OJ	*-gf* [OO½l
7i(T1.,1- T2.,-1)	10>,I-IJ,	*gf* +*[f,*[00 OJ	*[f,* [OO OJ	*-it* + *[f,* [O I OJ
-1(T1.,-1+ Ti.,,1)	II >ilOJ,	gf[OOO]	0 [I O OJ	*-it* [OO OJ
T2./J	:?!(II)il-1), - I-I)11I),)	gf [t O OJ	0 [O O OJ	*-gf* [OO½l
(T1.,1 +T2.,-1)	1-1)110),	gf[OOO]	0 [O O I]	*-it* [OO OJ

TABLE Ill. A list of theSO and DJT parameter values and their derivations from independently measured values assuming a *weak* DJT distortion.

Parameter	Value	**Relation tomeasured values**	**Measured values**	Refs.
it	2.242	EPR and magnetospectroscopy	2.242	**This work**
/iwpb	6.15THz	Optical spectroscopy	6.15 THz	[52]
{	-7.73 THz	f =*(go - Jf,)EPJlf4go*	*EPJI* = 258THz"	[43,45]
Err	0.26THz	*Err*= -(2/3) 1n(-612/{)	612 = 7.26 TH:t'	[65]
$\mu,$	4.92THz	$\mu,$ =(643+621+e-• ^{2}{/2- 3K1)/3e-•/2	643 = 12.6 THz"	[65]
p	-5.74 THz	*P* = -621- (I - *e-•1*^{2})$\mu,$ - *K2*	621 = 5.28 THz<l	[45]

a The'"oenter of mass"of the optical absorption line.

b Splitting between the *T2u* and *Ti.* lines.

c Splitting between the *A2.* and *T2.* lines.

d Splitting between the *Ti.* and *E.* lines.

and may be below the resolution limit. Similarly, Ll.43ss -Ll.$_{21}$- *i;e-•l*^{2} and becomes indiscernible from -Ll.$_{21}$. With these approximated values, one can see that μ, bas to be O and *p* bas to be -Ll.$_{21}$. All the other parameters are independent of the optical spectrum and can thus take the same values as in Table III.

We thus see that the same general model, though with differentµ,and *p* values, can fit the available spectroscopic data also if we assume that the DJT distortion is strong.

It is therefore impossible to discern between the case of a weak DJT distortion and that of a strong DJT distortion given only these data. For doing that, the additional measurements performed in this work were necessary.

APPENDIX C: ESEEMFORS = I AND/ =$_{5/2}$

The Hamiltonian for an electron-spilHluclear-spin interaction involving electron-spin states Zeeman split in a magnetic field along the *z* direction is diagonal in the electron-spin projection basis. For a given spin-projection value, *m,,* it can be written as [92,93]

$$Hm, = m,luvs - luv,I, + m,A,,I, + m,A,,I,, \tag{Cl}$$

where the magnetic field vector together with the vector pointing from the electron spin to the nuclear spin define the *x*-*z* plane.

Thus, when considering only the *m,* = - I lower state and them, = 0 upper state, which is a good approximation for the 9-mK experiment temperature, we obtain

$$H\text{-}1 = -luv,- (lilv1 + A,,)I, -A,,I,, \tag{C2}$$

and

$$Ho = -luv,I,. \tag{C3}$$

It is clear that while in the lower electron-spin state manifold there is coupling between the nuclear spin states, no such coupling is present in the higher electron-spin state manifold, where *m,* = 0, and the separation between the states in that manifold is determined only by the nuclear Zeeman frequency *w*$_1$, even if *A,,* and *A,,* are nonzero.

At the temperature of the experiment, while most of the population is in the ground electron-spin state, the nuclear spinstate is still fully mixed. Therefore, transitions starting in different ground states would not interfere. Hence, the frequencies of interference fringes are determined only by the frequency differences in the excited state and will therefore be harmonics of the nuclear Zeeman splitting. This is in striking contrast to the more commonly studied case of *m,* =±1/2 [92,93].

For a localized electron-spin with an isotropic *g* factor *gf* interacting with neighboring nuclear spins, the contact interaction is negligible and the components of the electron-spilHluclear-spin interaction tensor are given by the dipole-dipole interaction [93]

$$Ay = -\frac{3\mu o}{4{:}n lrl^5}\mu s\mu Ngfg.(lrl^2\, 8q - 3r,r_1), \tag{C4}$$

where μ_0 is the permeability of vacuum, μ,N and *g.* are the nuclear magneton and the nuclear *g* factor, respectively, and*r* is the position vector of the nuclear spin with respect to the electron spin. For MgO, the nearest Mgneighbors to the Ni substitutional site are located in all 12 permutations and sign combinations *ofr* =a(1/2, 0, 1/2), where *a* = 0.42 run is the lattice constant of MgO. The length of all these vectors is lrl= *a/.J'i.*. Outoftbe 12 possibilities, four do not contain the *z* component and for them *A,,* = 0, such that they will not exhibit any coupling between the different nuclear spin states and will not contribute to ESEEM. For the other eight,

$$A,, = \frac{3.J'i./J,o}{4na^3}/J,B/J,N\_gfg.,$$
$$A,, = \pm 3A,,. \tag{C5}$$

The minus sign in *A,,* appears in the four cases in which the *z* coordinate is negative with respect to the direction of the magnetic field. Using *Cn* = -0.34 for ^{25}Mg [126], we obtain *A,,/h* = 306 kHz and *Azx/h* = ±918 kHz, where *h* is Planck's constant. These values are comparable in absolute value to the nuclear Zeeman splitting at *B* = 141 mT and w_1/2n:= -366 kHz (here, the minus sign is due to the negative nuclear *g* factor), leading to a significant modulation depth. For the simple case of/ = 1/2, the visibility (which is only due to the nuclear spin state mixing in the *m,* = -l state), is given by [93]

$$V = P_{25} V_1, \tag{C6}$$

where

$$V_1 = \frac{|A_{zx}|/2}{\sqrt{(\hbar\omega_I + A_{zz})^2 + A_{zx}^2/4}} \tag{C7}$$

For the calculated interaction elements, Vi = 0.99. P_{25} is the probability that a magnesium atom within the region affecting the nickel ion will be ^{25}Mg. For example, if one considers only nearest neighbors, P_{25} = I - (I - *P2s)NM* = 0.57. Here, *Pis* = 0.1 is the natural abundance of ^{25}Mg and *Nnn* = 8 is the number of relevant nearest-neighbor sites. As not only nearest neighbors contribute, in practice this number may be effectively closer to I. The measured visibility at short times (before the onset of nuclear spin dephasing) is 0.75, which is in line with the above analysis.

As the nuclear spin of ^{25}Mg is S/2 and not l/2, additional modulation frequencies, harmonics of w_I up to the fifth harmonic, are possible. Indeed, this is seen in the measurement [Fig. 3(b)]. In order to calculate the ratios between the magnitude of the oscillations in the different frequencies, we numerically diagonalize the full / = S/2 Hamiltonian [Eq. (C2)], using the same parameter values as in Eq. (C7), and calculate the relative transition amplitudes using *S*, (the *x* component of the electron-spin) as the transition operator [92,93]. Then, for every ground state, we sum the amplitudes leading to all excited states and calculate the transition probability at each transition frequency for that ground state. Finally, we sum over the probabilities calculated in this way for all ground states. The result, including bandwidth limitations due to the pulse duration and cavity width, are presented by the yellow bars in Fig. 3(b).

In order to account for decoherence effects, we construct the temporal dependence of the transition probability from the result of the full / = S/2 model described above, *p(t),* and decompose it into its average value, Pmeao, and a purely oscillating component, p_0,c(t). We then produce the following function:

$$p_{\text{echo}}(t) = g_1(t)[p_{\text{mean}} + g_2(t)p_{\text{osc}}(t)], \tag{CB}$$

TABLE IV. The list of fit parameters for the spin-echo trace presented in Fig. 3(a).

Parameter	Value
A	0.917 ± 0.004
B	0.0825 ± 0.0005
P15	0.81 ± 0.005
-1	4.50 ± 0.03 μs
7f"81	109 ± 2 μs
r,.C•uc) 2	52 ± 2μs

where

g1(t) = Ae-1/1.,.,.> + *Be-vft"•>,*

g2(t) = P2se-•f1• >. (C9)

The result of fitting this function to the data is presented by the solid black line in Fig. 3(a). Note that here we have used the measured $|w_1$/2n:| = 385 MHz instead of the calculated value and we have used *Pis as* a fit parameter. Table IV presents the fitted parameter values.

APPENDIX D: SPECTRAL-DIFFUSION DEPBASING FOR S = I

Spectral diffusion of the probed spins can be caused by flip-flop processes within the surrounding spin bath, which stochastically change the magnetic field environment of the probed spins. The resulting dephasing rate is proportional to the number of spin pairs that can flip flop. As the flip-flop process conserves energy, one should count only the spin pairs in which the two spins have the same energy splitting. This number depends on the spin populations and hence depends on temperature, making the spectral-diffusion dephasing rate temperature dependent.

In order to find the temperature dependence, we first calculate the number of spin pairs at a given temperature, for a certain strain detuning of the *m,* = 0 level, *8*. We note that in a *S* = I system there are three possible flip-flop processes:

11,0) B- 10, I),

1- 1,0) B- 10,-1),

11,-1) B- 10,0), (DI)

where l*m,,*1, *m,,2)* represents a state of a spin pair in levels *m,,1* and *m,,2*• The numbers of spin pairs that conserve energy for these processes are, respectively,

n1(8)no(8),

n_1(8)no(8),

![n-1*(8)n1*(-8) + *no(8)no(-8)],* (02)

where *nm,* (o) is the nwnber of spins (per unit detuning) populating the level *m,* for a system with *m,* = 0 detuning of ***O.*** At a given temperature, the populations of the three levels are

n_,(o) oc 1/Z(o),

no(o) oc *e-P(ea-&)* /Z(o),

n,(o) oc e-^{2}'''• /Z(o),

where here /J = I/ *knT* is the inverse temperature in units of energy *(kn* is the Boltzmann constant) and *en* = *μ,₈B* is the Zeeman energy splitting. Z(o) = I + e-PC•a-&J + *e-*^{2}*/J•a* is the partition function. Note that here we have neglected anystrain shift of them, = I level.

The total spectral-diffusiondephasing rate is then given by swnming the nwnber of pairs for the three processes for a given *o,* multiplying by the detuning distribution function *P(o)* = *,T,na*J--e-^{82}l^{2}*a'* *(a* being the width of the distribution), and integratingover*o.* Alsoadding a temperature independent dephasing rate, representing the direct flip flop and instantaneous dilfusion processes, which are effectively constant at the (low) temperatures where they are significant, this yields

$$\frac{1}{T_2}=\frac{1}{T_{2,LT}}+\frac{3}{T_{2,SD,\mathrm{sat}}}\int_{-\infty}^{\infty}d\delta P(\delta)\times\left(\frac{e^{-\beta(\varepsilon_B-\delta)}+e^{-\beta(3\varepsilon_b-\delta)}}{Z^2(\delta)}+\frac{e^{-2\beta\varepsilon_B}}{Z(\delta)Z(-\delta)}\right), \quad (04)$$

where *T2,1.r* is the low-temperature dephasing time and *T2,so,sa,* is the spectral-dilfusion dephasing time at saturation (note that for low temperatures the integral tends to 0, while for high temperatures it tends to 1/J) and we have used the fact that *P(o)* is even.

For the fit used in Fig. 4, we use the measured values of *a*= 170 MHz and *e₈* = 4386 MHz *(B* = 141 mT) and fit the values of *T2,1,r* and *T2,so,sat*to the data. We obtain *T2,1,r* =85± 10 µ.s and *T2,so,,..* =2.65 ± 0.2 µs.

APPENDIX E: SPINg FACTOR IN THE ^{3}T2g(T,,) STATES

The SO interaction may alter the value of thespin *g* factor of a state by mixing it with other states of the same SO representation [99]. For the *T,.* SO states of the ^{3}*T2g* manifold, the closest such states are the *Tiu* SO states of the ^{3}T1g manifold. We thus asswne a wave function of the form

$$|\psi_j\rangle = N_j\left(|T_{1u,j}\rangle_{^3\mathrm{T}_{2g}}+\sum_{k=-1}^{1}\gamma_{k,j}|T_{1u,k}\rangle_{^3\mathrm{T}_{1g}}\right), \quad (E1)$$

where *Yt;* is the"mixing fraction" of thestate IT1u,t)1T,, in *t{,1* and = (I + Li:-t*Yi;*)-^{1}1^{2} is a normalization constant. Using second-order perturbation theory, the mixing fractions are given by

$$\gamma_{k,j}=\frac{{}_{^3\mathrm{T}_{2g}}\langle T_{1u,k}|H_{\mathrm{SO}}|T_{1u,j}\rangle_{^3\mathrm{T}_{1g}}}{E^{T_{1u}}_{^3\mathrm{T}_{1g}}-E^{T_{1u}}_{^3\mathrm{T}_{2g}}}, \quad (E2)$$

where *Hso* is the SO Hamiltonian and *E[T'•* *(E[T'''*) is the energy of the *T,.* states in the ^{3}T1g (3T2g) manifold. The effective *g* factor is then given by

$$g_{T_{1u}}=\frac{1}{\hbar}\langle\psi_1|L_z+g_0S_z|\psi_1\rangle. \quad (E3)$$

Using the known structure of the *Tiu* wave functions [125] and assuming that *Yt;* « I, one obtains

$$g_{T_{1u}}\approx\frac{1}{2}\left[g_L+g_0(1-2\gamma_{1,-1})\right], \quad (E4)$$

where *g₁,* = (T2g,,ILIT2g,₁) is calculated in Appendix F. Note that this calculation does not include DJT distortion. Its inclusion amounts to replacing *gL* with*CL·* By means of Table I, we identify

$$g^{e}_{s}=g_0(1-2\gamma_{1,-1}). \quad (E5)$$

Using *E[. -E[* =160 THz [65], *'Tz.*(Ttu,tlHsol *TtuJ*),T,, =-4-S [125,127], and the value of S extracted from the *g* factor of the ground state (Appendix B), S = -7.73 THz, we obtain Y1,-1 =0.04, yieldingg; = 1.84.

APPENDIX F: ORBITALg FACTOR IN THE ^{3}T2g MANIFOLD

In the *d8* configuration, it is much easier to use the hole notation, as then one has to consider only the two empty electron orbitals instead of the eight full ones. We therefore first find the orbital angular momentum of the two-electron orbitals from which electrons are missing and then take the negative of the result, as we are interested in the orbital angular momentum of a full shell (which is 0) *minus* those two electrons.

All the relevant two-electron orbitals are composed mostly of products of two *d* (*l* =2) single-electron states. Therefore, they are mostly composed of doubly quadratic functions of the Cartesian coordinates.

For spin-triplet states, which are exchange symmetric, the orbitals also have to be exchange antisymmetric, as the total electronic wave function must be exchange antisymmetric.

Out of all the possible T*2g* two-electron orbitals, we focus here on those in which one electron is of the *eg* single-electron orbital and the other is of the t_{2g} single-electron orbital (see Fig. I(b)].

Therefore, we have to use a set of spanning functions of the T_{2g} representation of the *Oh* point group, which are doubly quadratic in *x, y,* and *z,* are composed of products of quadratic basis functions of the Eg and T_{2g} representations, and are exchange antisymmetric.

These constraints leave only one possible choice (up to internal unitary transformations). Choosing the main axis to be *z* and all the functions to be eigenfunctions of the *z* component of the angular momentum, we are left with (125]

IT2g,1). = -:Ji{X1Z1*(3y]* - *ri>*+ iY1Z1(3 - *ri))* ,

IT2g,o)e = ia{x1y1(3zJ-ri)la.s.,

IT2g,-1)e = ,12{X1Z1*(3y]* - ri) - iy1z1(3.>:i- ri))u,

(FI)

where the subscript *e* indicates that these are electronic orbitals, { }a.s. stands for exchange antisymmetri7.ation, *r;*<₂>=xf(2) +*Yf*<2>+ (2)• and *a*= 5/(4n.J'i.) is a normalization constant.

By inverting the definitions of the spherical harmonics in Cartesian coordinates, it can be shown [125] that these functions can be represented as the following combinations of products of single-electron *d* orbitals:

IT2g,1). = li<l1, 2) + 11, -2)) - ½1-1, 0))…. ,

IT2g,o). = }i!l2,0) -1-2,0)Ja.,,

IT2g,-1). = -li<1-1,2) + I-I,-2))-½II,0))a.s.,

(F2)

where the twonumbers inthe kets stand for theeigenvalues of the *z* component of the angular momentum of the single-electron *d* orbitals of the two electrons.

With the wave functions cast in this form, it is straightforward tocalculate their two-electron angular-momentum matrix elements. One obtains

I

(L,) = .*Jj*i'*i*. (0₁ 0 !')
2 2 O

(F3)

–i

(L,,) = .*Jj*i'*i*. (0ᵢ 0
2 2 O i /)'

(F4)

O

(L,) = -*Ii* (0 0) -
2 0 0 -I

(F5)

It is clear that these are spin-I matrices, as expected, just multiplied by a common factor of l/2. Thus, one can treat the T_{2g} two-electron orbitals as an effective I = 1 system, with an effective orbital *g* factor of 1/2.

Now, recall that we are interested in the orbital angular momentum of a full *d* shell *missing* two electrons in the above states. Weshould therefore take the *negative* of the above result; i.e.,

$$g_L = -1/2. \tag{F6}$$

[I] H. J. Kimble, The quantum Internet, Nature 453, 1023 (2008).

[2] T. Zhongand P. Goldner, Emerging rare-earth doped mate**rial platforms forquantumnanophotonics,** Nanophotonics **8,** 2003 (2019).

[3] G. Wolfowicz, F. J. Heremans, C. P. Anderson, S. Kanai, H. Seo, A. Gali, G. Galli, and D. D. Awschalom, Qubit **guidelines for solid-state spin defects,** Nat. Rev. Mater. 6, 906(2021).

[4] G. Balasubramanian, P. Neumann, D. Twitchen, **M.** Markham, R. Kolesov, N. Mizuochi, J. lsoya, J. Achard, **J. Beck, J. Tissler, V. Jacques, P. R. Hemmer, F. Jelezko, and J. Wrachtrup, UJtralong spin coherence time in** is topically engineered diamond, Nat. Mater. 8, 383 (2009).

[5] K. Saeedi, S. Simmons, J. Salvail, P. Dluhy, H. Riemann, N. Abrosimov, P. Becker, H.-J. Pohl, J. Morton, and **M. Thewalt, Room-temperature quantum bit storage exceeding 39 minutesusing ionizeddonorsin silicon-28,** Science 342, 830(20 I3).

[6] N. Bar-Gill, L. M. Pham, A. Jarmola, D. Budker, and R. **L. Walsworth, Solid-state electronic spin coherence time** approaching one second, Nat. Commun. **4,** 1743 (2013).

[7] M. Zhong, **M.** P. Hedges, R- L. Ahlefeldt, J. G. Bartholomew, S. E. Beavan, S. M. Wittig, J. J. Longdell, and M. J. Sellars, Optically addressable nuclear spins in **a solid with a six-hour coherence time, Nature 517, 177** (2015).

[8] C. Cohen-Tannoudji, J. Dupont-Roe, and G. Gtynberg, in *Atom-Photon Interactions* (John Wiley & Sons, Ud, New York, I998), Chap. I, p. *5.*

[9] G. Corrielli, A. Seri, M. Mazzera, R. Osellame, and H. de Riedmatten, Integrated optical memory basedon laser-written waveguides, Phys. Rev. Appl. 5, 0540I3 (20 I6).

[IOJ P. R. Hemmer, A. V. Turukhin, M. S. Shahriar, and J. **A. Musser, Raman-excited spin coherences in nitrogen-**vacancy color centers in diamond, Opt. Lett. 26, 36 I (2001).

[11J S. Rand, A. Lenef, and S. Brown, Zeeman coherence and quantum beats in ultrafast photon echoes of N-V centers in diamond, J. Lumin. 60-61, 739 (1994).

[12] A. Lenef, S. W. Brown, D. A. Redman, S. C. Rand, J. Shigley, and E. Fritsch, Electronic structure of the N-V center in diamond: Experiments, Phys. Rev. B 53, 13427 (1996).

[13] B. Zhou, A. Baksic, H. Ribeiro, C. Yale, F. Heremans, P. Jerger, A. Auer, G. Burkard, A. Clerk, and D. Awschalom,

Accelerated quantum control usingsuperadiabatic dynamics in a solid-state lambda system, Nat. Phys. I3, 330 (2017).

(14] C. Weinzetl, J. Gorlitz, J. N. Becker, I. A. Walmsley, E. Poem, J. Nunn, and C. Becher, Coherent control and wave mixing in ensemble of Silicon Vacancy centers in diamond, Phys. Rev. Lett. 122, 063601(2019).

[15] H. Zu, W. Dai, and A. de Waele, Development of dilution refrigerators--a review, Cryogenics 121, 103390 (2022).

[16] T. Bottger, C. W. Thiel, R. L. Cone, and Y. Sun, Effects of magnetic field orientation on optical decoherence in Er3+:Y2SiOs, Phys. Rev. B 79, 115104 (2009).

[17] C. Thiel, R. Macfarlane, T. Bottger, Y. Sun, R. Cone, and W. Babbitt, Optical decoherence and persistent spectral hole burning in Er3+:LiNb03, J. Lumin. 130, 1603 (2010).

[18] M. Rancic, M. P. Hedges, R. L. Ahlefeldt, and M. J. Sellars, Coherence time of over a second in a telecom-compatible quantum memory storage material, Nat. Phys. 14, 50 (2018).

[19] M. W. Doherty, N. B. Man.son, P. Delaney, F. Jelez.ko, J. Wrachtrup, and L. C. Hollenberg, The nitrogen-vacancy colour centre in diamond, Phys. Rep. 528, I (2013).

[20] E. Togan, Y. Chu, A. S. Trifonov, L. Jiang, J. Maze, L. Childress, M. V. G. Dutt, A.S. Sorensen, P. R. Hemmer, A. S. Zibrov, and M. 0. Lukin, Quantum entanglement between an optical photon and a solid-state spin qubit, Nature 466, 730 (20JO).

[21] C. G. Yale, B. B. Buckley, D. J. Christle, G. Burkard, F. J. Heremans, L. C. Bassett, and D. D. Awschalom, All-optical control of a solid-state spin using coherent dark states, Proc. Natl. Acad Sci. 110, 7595(2013).

[22] D. A. Goiter and H. Wang, Optically driven Rabi oscillations and adiabatic passage of single electron spins in diamond, Phys. Rev. Lett. II 2, 116403 (2014).

[23] B. Hensen, H. Bemien, A. E. Dreau, A. Reiserer, N. Kalb, M. S. Blok, J. Ruitenberg, R. F. Vermeulen, R. N. Schouten, C. Abellan, W. Amaya, V. Pruneri, M. W. Mitchell, M. Markham, D. J. Twitchen, D. Elkouss, S. Wehner, T. H. Taminiau, and R. Hanson, Loophole-free Bell inequality violation usingelectron spins separated by 1.3 kilometres, Nature 526,682 (2015).

[24] B. B.Zhou, P.C. Jerger, V.0. Shkolnikov, F. J. Heremans, G. Burkard, and D. D. Awschalom, Holonomic quantum control by coherent optical excitation in diamond, Phys. Rev. Lett. I19, 140503 (2017).

[25] D.Chen, N. Zheludev, and W.-B. Gao, Building blocksfor quantum network based ongroup-IV split-vacancy centers in diamond, Adv. Quantum Technol. 3, 1900069 (2020).

[26] C. W. Thiel, T. Bottger, and R. L. Cone, Rare-earth-doped materials forapplications in quantum infonnation storage and signal processing, J. Lumin. 131,353(2011).

[27] H.-J. Lim, S. Welinski, A. Ferrier, P. Goldner, and J. J. L. Morton, Coherent spin dynamics of ytterbium ions in yttrium orthosilicate, Phys. Rev. B 97, 064409 (2018).

[28] R. de Biasi and M. Grillo, Influence of gadolinium concentration on the ESR spectrum of Gd^3+ in MgO, J. Phys. Chem.Solids 65, 1207(2004).

[29] A. E. Hughes and G. P. Pelis, Fluorescence spectra of Gd^3+ ions in CaO, J. Phys. C: Solid State Phys. 7, 3997 (1974).

[30] H. Ebendorff-Heide riem and D. Ehrt, Electron spin resonance spectra of Eu + and Tb<+ ions in glasses, J. Phys.: Condens. Matter 11, 7627(1999).

[31] Z. Pan, L. Ning, B.-M. Cheng, and P.A. Tanner, Absorption, excitation and emission spectra of $StCii:Eu^2+$, Chem. Phys. Lett. 428, 78 (2006).

(32) R. Verma, K. Kumar, and S. Rai, Inter-conversion of To^3+ and Th^4+ states and its fluorescence properties in MO-A'20J: Tb (M=Mg, Ca, Sr, Ba) phosphor materials, Solid State Sci. 12, 1146 (2010).

[33] M. lllemassene, N. Edelstein, I<.Murdoch, M.Karbowiak, R. Cavellec, and S. Hubert, Site-selective spectroscopy and crystal field analysis of Cm^3+ diluted in CsCdBr3, J. Lumin. 86, 45 (2000).

[34] L. Shang, Q. Chen, W. Jing, C.-G. Ma, C.-K. Ouan, and J. Du, First-principles study of transition metal dopants as spin qubits, Phys. Rev. Mater. 6, 08620I (2022).

[35] T. Bosma, G. J. Lof, C. M. Gilardoni, 0. V. Zwier, F. Hendriks, B. Magnusson, A. Ellison, G. andreas, I. G. Ivanov, N. T. Son, R. W. Havenith, and C. H. van der Wal, Identificationand tunable optical coherent control of transition-metal spins in siliconcarbide, Npj Quantum [nf. 4, I (2018).

[36] C. M. Gilardoni, T. Bosma, D. van Hien, F. Hendriks, B. Magnusson, A. Ellison, I. G. Ivanov, N. T. Son, andC. H. van der Wal, Spin-relaxation times exceeding seconds for color centers with strong spin-orbit coupling in sic, New J. Phys. 22, I03051 (2020).

[37] G. Wolfowicz, C. P. Anderson, B. Oiler, 0. G. Poluektov, F. J. Heremans, and D. D. Awschalom, Vanadiumspin qubits as telecom quantum emitters in siliconcarbide, Sci. Adv. 6, eaazl192 (2020).

[38] T. Astner, P. Koller, C. M. Gilardoni, J. Hendriks, N. T. Son, I. G. Ivanov, J. U. Hassan, C. H. van der Wal, and M. Trupke, Vanadium in silicon carbide: Telecom-ready spin centres with long relaxation lifetimes and hyperfine-resolved optical transitions, arXiv:2206.06240 (2022).

[39] W. F. Koehl, B. Oiler, S. J. Whiteley, A. Bourassa, N. T. Son, E. Janzen, and D. D. Awscha)om, Resonant optical spectroscopy and coherent control of Cr"+ spin ensembles in SiC and GaN, Phys. Rev. B 95, I (2017).

[40] B. Oiler, S. J. Whiteley, C. P. Anderson, G. Wolfowicz, M. E. Wesson, E. S. Bielejec, J. F. Heremans, and D. D. Awschalom, Coherent control and high-fidelity readout of chromium ions in commercial silicon carbide, npj Quantum Inf. 6, 11(2020).

[41] W. Low, Paramagnetic and optical spectra of divalent nickel in cubic crystalline fields, Phys. Rev. 109, 247 (1958).

[42] J. W. Orton, P. Auzins, and J. E. Wertz, Double-quantum electronspinresonance transitionsof nickel in magnesium oxide, Phys. Rev. Lett. 4, 128(1960).

[43] W. M. Walsh, Effects of hydrostatic pressure on the paramagnetic resonance spectra of several iron group ions in cubic crystals, Phys. Rev. 122,762 (1961).

[44] J. W. Orton, P. Auzins, and J. E. Wertz, Estimate of the nuclear moment of Ni^{61} from electron spin resonance, Phys. Rev. 119, 1691 (1961).

[45] R. Pappalardo, D. L. Wood, and R. C. Linares, Optical absorption spectra of Ni-doped oxide systems. I, J. Chem. Phys. 35, 1460 (1961).

[46] S. Minomura and H. G. Drickamer, Effect of pressure on the spectra of transition metal ions in MgO and A'2O3, J. Chem. Phys. 35,903 (1961).

[47] M. F. Lewis and A. M. Stoneham, Temperature dependence of the spin-lattice relaxation times of Fe++ and Ni++ in MgO, Phys. Rev. 5, *595* (1967).

[48] J. B. Jones and M. F. Lewis, Interaction of microwave phonons with iron-group ions Fe^{2+} and, Ni^{2+} in magnesium oxide, Solid State Commun. I64, 762 (1967).

[49] J. E. Ralph and M. G. Townsend, Near-infrared fluorescence and absorption spectra of Co^{2+} and Ni^{2+} in MgO, J. Chem. Phys. **48,** 149(1968).

[50] S. R. Smith, F. Oravnieks, and J. E. Wertz, Electron-paramagnetic-resonance line shapeofNi^{2+} in MgO, Phys. Rev. 178,471(1969).

[51] J. E. Ralph and M. G. Townsend, Fluorescence and absorption spectra of Ni^{2+} in MgO, J. Phys. C: Solid State Phys. 3, 8 (1970).

[52] N. B. Manson, One-phonon vibronic transition $^3T_{2g}$-$^3A_{2g}$ ofNi^{2+} in MgO, Phys. Rev. B 4, *2645* (1971).

[53] M. J. L. Sangster and C. W. McCombie, Calculation of phononsidebands in emissionspectra of V^{2+} and Ni^{2+} in MgO, J. Phys. C: Solid State Phys. 3, 1498 (1970).

[54] B. 0. Bird, G. A. Osborne, and P. J. Stephens, Magnetic circular dichroism of impurities in solids: Vibrationally induced d d transitions in MgO:Ni, Phys. Rev. B 5, 1800 (1972).

[55] I<. Y. Wong, D. Sengupta, and E. R. Krausz, Magnetic circular dichroism of the $^3A_{2g}{}^3T_{2g}$ band of Mg0-Ni^{2+}, Chem. Phys. Lett. 21, 137 (1973).

[56] N. Moreau, A. C. Boccara, and J. Badoz.,Jahn-Teller effect and relaxation processes inthe $^1T_{2g}$ state of Ni^{2+} in MgO, Phys. Rev. B I0, 64 (1974).

[57] N. Manson, Electron-vibration splitting of the vibronic levelss of the $^1T_{2g}$ state of Mg0:Ni^{2+}, Solid State Commun. 18,257 (1976).

[58] J. S. Thorp and M. 0. Hossain, ESR linewidth mechanisms in Ni^{2+}JMgO, J. Mago. Mago. Mater. 22, 311 (1981).

[59] S. A. Payne, Energy-level assignments for the ^1E and ^3T1a states of MgO:Ni^{2+}, Phys. Rev. B 41, 6109 (1990).

[60] C. Campochiaro, D. S. McClure, P. Rabinowitz, and S. Dougal, Two-photon spectroscopy of MgO:Ni^{2+}, Phys. Rev. B 43, 14(1991).

[61] N. Mironova, A. Kuzmin, J. Purans, and A. Rodionov, X-ray absorption spectroscopy studies of the off-center Ni^{2+} ions in Ni,Mg1-,O solid solutions, Proc.SPJE-Int. Soc. Opt. Eng. 2706, 168(1996).

[62] N. Mironova-Ulmane, M. G. Brik, and I. Sildos, Crystal field calculations of energy levels of the Ni^{2+} ions in MgO, J. Lumin. 135,74 (2013).

[63] P. F. Moulton and A. Mooradian, Broadly tunable cw operation of Ni:MgF2 and Co:MgF2 lasers, Appl. Phys. Lett. 35,838 (1979).

[64] M. V. Iverson, J.C. Windscheif, and W. A. Sibley, Optical parameters for the Mg0:Ni^{2+} laser system, Appl. Phys. Lett. 36, 183(1980).

[65] R. Moncorge and T. Benyattou, Excited-state absorption ofNi^{2+} in MgF2 and MgO, Phys. Rev. B 37, 9186 (1988).

[66) G. D. Cheng, L. Yan, and Y. Chen, Divalent nickel-doped cubic magnesium oxide for spin qubitapplication, J. Mater.Sci. 52, 8200 (2017).

[67] S. Kanai, F. J. Heremans, H. Seo, G. Wolfowicz, C. P. Anderson, S. E. Sullivan, M. Onizhuk, G. Galli, 0. D. Awscha)om, and H. Ohno, Generalized scaling of spin qubit coherence in over 12,000 host materials, Proc. Natl. Acad.Sci. 119, e212 I808ll 9 (2022).

[68] E. J. Catanzaro, T. J. Murphy, E. L. Gamer, and W. R. Shields, Absolute isotopic abundance ratios and atomic weight of magnesium, J. Res. Natl. Bur. Stand. A 70A, 453 (1966).

[69] F. S. Ham, Dynamical Jahn-Teller effect in paramagnetic resonance spectra: Orbital reduction factorsand partial quenching of spin-orbit interaction, Phys. Rev. 138, A1727(1965).

[70] H. M. Rosenberg and J. K. Wigmore, Acoustic paramagnetic resonance ofNi^{2+} in potassiummagnesiumfluoride, Proc. Roy. Soc. A. 302, 69 (1967).

[71] R. D. Mattuck and M. W. P. Srandberg, Spin-phonon interaction in paramagnetic crystals, Phys. Rev. 119, 1204 (1960).

[72] W.-C. Zheng, Theoretical calculations of the spin-lattice coupling coefficients G11and *G.,* for MgO:Ni^{2+} crystals, Phys. Rev. B 40, 7292 (1989).

[73] O.-P. Ma, N. Ma, X.-O. Ma, and H.-M. Zhang, Energy spectrum and g fuctor of Mg0:Ni^{2+} and their pressure-induced shift, J. Phys. Chem Solids 59, 1211 (1998).

[74] U. Kaufmann, P. Koidl, and 0. F. Schirmer, Near infrared absorption ofNi^{2+} in ZnO and ZnS: Dynamic Jahn-Teller effect in the $^3T2$ state, J. Phys. C: Solid State Phys. 6,310 (1973).

[75] Y. Kodriano, I. Schwartz, E. Poem, Y. Benny, R. Presman, T. Truong, P. Petroff, and D. Gershoni, Complete control of a matter qubit using a single ps-laser pulse, Phys. Rev. B 85, 241304(2012).

[76] K. Heshami, C. Santori, B. Khanaliloo, C. Healey, V. M. Acosta, P. E. Barclay, and C. Simon, Raman quantum memory based on an ensemble of nitrogen-vacancy centers coupled to a microcavity, Phys. Rev. A 89, 040301 (2014).

[77] G. Buser, R. Mottola, B. Cotting, J. Wolters, and P. Treutlein, Single-photon storage in a ground-state vapor cell quantum memory, PRX Quantum 3, 020349 (2022).

[78] E. Poem, C. Weinzetl, J. Klatzow, K. T. Kaczmarek, J. H. D. Munns, T. F. M. Champion, D. J. Saunders, J. Nunn, and I. A. Walmsley, Broadband noise-free optical quantum memory with neutral nitrogen-vacancy centers in diamond, Phys. Rev. B **91**, 205!08 (2015).

[79] G. Walker, B. Kamaluddin, T. Glynn, and R. Sherlock, Luminescence of Ni^{2+} centers in forsterite (Mg2Si04), J. Lumin. 60-61, 123(1994).

[80] U. Kaufmann, H. Ennen, J. Schneider, R. Womer, J. Weber, andf. Kohl, Spectroscopic study of vanadium in GaP and GaAs, Phys. Rev. B 25, *5598* (1982).

[81] B. Lambert, B. Deveaud, Y. Toudic, G. Pelous, J.C. Paris, and G. Crandpierre, Properties of vanadium in JnP, Solid State Cornmunications 47, 337(1983).

[82] G. Annelles, J. Barrau, and D. Thebault, Uniaxial-stress spectroscopy ofluminescenoe at 0.74 eV from vanadium-doped gallium arsenide, J. Phys. C: Solid Stale Phys. 17, 6883 (1984).

[83] G. Annelles, J. Barrau, D. Thebault, and M. Brousseau, Zeeman spectroscopy of luminescence from vanadium doped gallium arsenide, J. Phys. 45, 1795 (1984).

[84] W. Ulrici, K. Friedland, L. Eaves, and D. P. Halliday, Optical and electrical properties of vanadium-doped GaAs, Phys. Status Solidi (b) 131, 719 (1985).

[85] W. Ulrici, K. Friedland, L. Eaves, and D. P. Halliday, Optical studies of vanadium in gallium phosphide, Phys.Status Solidi (B) 141,191(1987).

[86] A. M. Hennel, C. D. Brandt, K_ Y. Ko, J. Lagowski, and H. C. Gatos, Optical and electronic properties of vanadium in gallium arsenide, J. Appl. Phys. 62, 163 (1987).

[87] A. Gorger, B. K. Meyer, J. M. Spaeth, and A. M. Hennel, Identification of spin, charge states and optical transitions of vanadium impurities in GaAs, Semicond. Sci.Technol. 3,832 (1988).

[88] J. J. Chen and M. L. Du, Investigation of the optical spectra and EPR parameters of vanadium in IH-V semiconductors (GaAs, GaP, lnP), Phys. B: Condens. Matter 291, 270(2000).

[89] A. Bchetnia, A. Rebey, J. C. Bourgoin, and B. Eljani, A study of deep levels in vanadium-doped GaAs grown by OMVPE, Semicond. Sci. Technol. 18,445 (2003).

[90] R. Heitz, A. Hoffinann, B. Hausmann, and I. Broser, Zeeman spectroscopy ofV^{3}+-tuminescenceinZnO, J. Lumin. 48-49, 689 (1991).

[911 R. L. Hartman, J. S. Bennett, J. G. Castle, Jr., Spin relaxation of cr3+ in MgO: Evidence for localized modes, Phys. Rev. B 1, I946 (I970).

[92] L. G. Rowan, E. L. Hahan, and W. B. Mims, Electron-spin-echo envelope modulation, Phys. Rev. 137, A61 (1965).

[93] S. Probst, G. Zhang, M. RanCiC, V. Ranjan, M. Le Dantec, Z. Zhang, B. Albanese, A. Doll, R- B. Liu, J. Morton, T. Chaneliere, P. Goldner, D. Vion, D. Esteve, and P. Bertel, Hyperfine spectroscopy in a quantum-limited spectrometer, Mago. Reson. 1, 315 (2020).

[94] E. Dikarov,0. Zgadzai, Y. Artzi, and A. Blank, Direct measurement of the flip-flop rate of electron spins in the solid stale, Phys. Rev. Appl. 6, 04400I (2016).

[95] M. RanCiC, M. Le Dantec, S. Lin, S. Bertaina, T. Chaneliere, D. Serrano, P. Goldner, R. 8. Liu, E. Flurin, D. Esteve, D. Vion, and P. Bertel, Electron-spin spectral diffusion in an erbium doped crystal al millikelvin temperatures, Phys. Rev. B 106, 144412 (2022).

[96] J. Alexander, G. Dold,0. W. Kennedy, M. Simimas, J. O'Sullivan, C. W. Zollitsch, S. Welinski, A. Ferrier, E. Lafitte-Houssal, T. Lindstrom, P. Goldner, and J. J. L. Morton, Coherent spin dynamics of rare-earth doped *crystals* in the high-cooperativity regime, Phys. Rev. B 106, 245416 (2022).

[97] S. Shankar, A. M. Tyryshkin, J. He, and S. A. Lyon,Spin relaxationand coherence times forelectronsatthe Si/Si02 interface, Phys. Rev. B 82, 195323 (2010).

[98] G. F. lmbusch, W. M. Yen, A. L. Schawlow, D. E. McCumber, and M. D. Sturge, Temperature dependence of the width and position of the ^{2}E ^{2}A, fluorescence lines ofcr3+ and V^{2}+ in MgO, Phys. Rev. 133, Al029 (1964).

[99] A. A. Misetich and T. Buch, Gyromagnetic factors and spin-orbit coupling in ligand field theory, J. Chem. Phys. 41, 2524(1964).

[100] D. Press, T. D. Ladd, B. Zhang, and Y. Yamamoto, Complete quantum control of a single quantum dot spin using ultrafast optical pulses, Nature 456, 218 (2008).

[IOI] E. Poem, 0. Kenneth, Y. Kodriano, Y. Benny, S. Khatsevich, J. Avron, and D. Gershoni, Optically induced rotation of exciton spin in a semiconductor quantum dot, Phys. Rev. Lett. 107, 087401 (201I).

[102] C. Simon *et al.,* Quantum memories, Eur. Phys. J. D 58, I (2010).

[I03] K. Heshami, D. G. England, P. C. Humphreys, P. J. Bustard, V. M. Acosta, J. Nunn, and B. J. Sussman, Quantum memories: Emerging applications and recent advances, J. Moel Opt. 63, 2005 (2016).

[I04] J. Nunn, I. A. Walmsley, M. G. Raymer, I<- Sunnacz, F. C. Waldermann, Z. Wang, and D. Jaksch, Mappingbroadband single-photon wave packets into an atomic memory, Phys. Rev. A 75, 01140 I (2007).

[I05] 0. Lahad and0. Firstenberg, Induced cavities for pholonic quantum gates, Phys. Rev. Lett. 119, 113601(2017).

[106] J. Nunn, J. Munns, S. Thomas, K. Kaczmarek, C. Qiu, A. Feizpour, E. Poem, 8. Brecht, D.Saunders, P. Ledingham, D. Reddy, M. Raymer, and I. Walmsley, Theory of noise suppression in A-type quantum memories by means of a cavity, Phys. Rev. A 96, 012338 (2017).

[I07] D. J. Saunders, J. H. D. Munns, T. F. M. Champion, C. Qiu, K. T. Kaczmarek, E. Poem, P. M. Ledingham, I. A. Walmsley, and J. Nunn, Cavity-Enhanced Room-Temperature Broadband Raman Memory, Phys. Rev. Lett. 116, 09050I (2016).

[I08] P. S. Michelberger, T. F. M. Champion, M. R.Sprague, I<- T. Kaczmarek, M. Barbieri, X. M. Jin, D. G. England, W. S. Kolthammer, D. J. Saunders, J. Nunn, and I. A. Walmsley, Interfacing GHz-bandwidth heralded single photons with a warm vapour Raman memory, New J. Phys. 17, 043006(20 I5).

[109] K. F. Reim, P. Michelberger, K. C. Lee, J. Nunn, N. I<-Langford, and I. A. Walmsley, Single-photon-level quantum memory at room temperature, Phys. Rev. Lett. 107, 053603(20 II).

[I10]S. E. Thomas, T. M. Hird, J. H. D. Munns, B. Brecht, D. J. Saunders, J. Nunn, I. A. Walmsley, and P. M. Ledingham, Raman quantum memory with built-in suppression of four-wave-mixing noise, Phys. Rev. A 100, 033801 (2019).

[111] 0. Davidson, 0. Yogev, E. Poem, and0. Firslenberg, Fast, noi free atomic optical memory with 35% end-to-end efficiency, arXiv:2212.04263 (2022).

[I12] R- Finkelstein,0. Lahad,0. Michel,0. Davidson, E. Poem, and 0. Firstenberg, Power narrowing:Counteracting doppler broadening in two-color transitions, New J. Phys. 21, I03024 (20 I9).

[I13] R- Finkelstein, 0. Lahad, I. Cohen, 0. Davidson, S. Kiriati, E. Poem, and 0. Firstenberg, Continuous protection of a collective state from inhomogeneous dephasing, Phys. Rev. X 11, 011008 (2021).

[114) V. Damon, M. Bonarota, A. Louchet-Chauvet, T. Chaneliere, and J.-L. L. Gouet, Revival of silenced echo and quantum memory for light, New J. Phys. 13, 093031 (2011).

[I 15) D. Farfumik, Y. Horowicz, and N. Bar-Gill, Identifying and decoupling many-body interactions in spin ensembles in diamond, Phys. Rev. A 98, 033409(2018).

[116) S. Gupta, X.Wu, H. Zhang, J. Yang, and T. Zhong, Robust millisecond coherence times of erbium electron spins, Phys. Rev. Appl. 19, 044029 (2023).

[117) P. London, J. Scheuer, J.-M. Cai, I. Schwarz, A. Retzker, M. 8. Plenio, M. Katagiri, T. Teraji, S. Koizumi, J. (soya, R. Fischer, L. P. McGuinness, B. Naydenov, and F. Jelez.ko, Detecting and polarizfog nuclear spins with double resonance on a single electron spin, Phys. Rev. Lett. 111, 067601 (2013).

[118) 0. Katz, R. Shaham, E. S. Polzik, and 0. Firstenberg, Long-lived entanglement generation ofnuclearspins using coherent light, Phys. Rev. Lett. 124,043602 (2020).

[119) H. P. Bartling, M. H. Abobeih, B. Pingault, M.J. Degen,S. J. H. Loenen, C. E. Bradley, J. Randall, M. Markham, D. J. Twitchen, and T. H. Taminiau, Entanglement of spin-pair qubits with intrinsic dephasing times exceeding a minute, Phys. Rev. X 12, 011048 (2022).

[120) P. Koidl, F. Schirmer, and U. Kaufmann, Near infrared absorption ofCn^{2+} in ZnS: Weak Jahn-Teller coupling in the ^{4}T2 and ^{4}T1states, Phys. Rev. B 8, 4926 (I 973).

[121) P. Thurian, R. Heitz, A. Hoflinann, and I. Broser, Nonlinear Zeeman effect of the Nil+ centre in ZnO, J. Cryst. Growth. 117,727 (1992).

[122) T. C. Brunold, A. Hauser, and H. U. Gtidel, Absorption and luminescence spectroscopy of ferrate (VI) doped into crystals ofK2MO, (M =S, Se, Cr, Mo), J. Lumin. 59,321 (1994).

[123) D. Ammerlahn, B. Clerjaud, D. Cote, L. Kohne, M. Krause, and D. Birnberg, Spectroscopic investigation of neutral niobium in GaAs, Mater. Sci. Forum 258-263, 911 (1997).

[124) V. V. Ushakov, D. F. Aminev, and V. S. Krivobok, Intracenter radiative transitions at tantalum impurity centers in cadmium telluride, Semiconductors 52, 1686(2018).

[125) J. S. Griffith, The *Theory of Transition-Meta/ Ions* (Cambridge University Press, Cambridge, I961).

[126) P. Raghavan, Table of nuclear moments, At. Data Nucl. Data Tables 42, 189(1989).

[127) A. D. Liehr and C. Ballhausen, Complete theory ofNi(II) and V(UI) in cubic crystalline fields, Ann. Phys. (NY) 6, 134 (1959).